Journal of Sound and Vibration (1999) **228**(4), 793–836
Article No. jsvi.1999.2441, available online at http://www.idealibrary.com on IDEAL®

DESIGN SELECTION AND ANALYSIS OF A SWEPT AND LEANED STATOR CONCEPT

E. ENVIA

Acoustics Branch, NASA Glenn Research Center, Cleveland, OH 44135, *U.S.A.*

AND

M. NALLASAMY

Aeromechanics Department, DYNACS Engineering Co., Inc. Brook Park, OH 44142, *U.S.A.*

(*Received* 9 *December* 1998, *and in final form* 3 *June* 1999)

This paper describes a two-part analytical study of the benefits of stator sweep and lean for reducing rotor-stator interaction tone noise. The first part of the paper describes a design study aimed at selecting a sweep and lean configuration that maximizes noise reductions for a candidate low-noise stator. In the second part, the predicted noise reductions that can be achieved by such a stator are compared with its measured benefits.

The results from the first part indicate that the kinematic relationship between the rotor wakes and stator vanes is the principal factor in determining the achievable noise reductions. It is shown that properly chosen sweep and lean enhance wake tilting as seen by the stator vanes. This, in turn, increases the number of wake intersections per vane leading to reduced noise levels. This argument suggests that to reduce noise, sweep and lean must be chosen in such a way that the number of wake intersections per vane is increased. Thus, a simple design rule is proposed for implementing sweep and lean. To achieve significant noise reductions, the rule calls for a sweep configuration for which vane tip is downstream of its root and vane lean that is in the direction of the rotor rotation.

In the second part of the study, a detailed assessment of the acoustic performance of the swept and leaned stator is carried out by comparing its predicted and measured noise reductions. Overall, these comparisons show that the predicted benefits of the swept and leaned stator are in good agreement, qualitative as well as quantitative, with the measured reductions for the fan speeds that are relevant to the standard noise certification procedures. Furthermore, the results demonstrate the validity of the design criterion as well as the theoretical tools used in the design and analysis phases of this study.

1. INTRODUCTION

The commercial air traffic is expected to increase substantially in the coming years as air travel becomes more affordable worldwide. At the same time, increasingly more stringent community noise regulations continue to place severe limits on the acceptable level of aircraft noise near airports. To address these concerns and

0022-460X/99/490793 + 44 $30.00/0

develop low-noise propulsion technologies, promising concepts for suppression of noise emissions from subsonic aircraft are being investigated under the auspices of NASA Advanced Subsonic Technology (AST) initiative. The AST requirements call for a 10-dB reduction in the aircraft's effective perceived noise level (EPNL) by the end of this decade [1]. Such dramatic reductions demand a comprehensive and systematic approach to the problem of noise suppression and require a better understanding of the noise generation processes through both theoretical and experimental studies. Fortunately, the essentially additive nature of aircraft noise sources allows the individual sources to be targeted separately which significantly reduces the complexity of problem.

The study reported here focuses on the reduction of fan-associated noise, which is known to be a major source of modern aircraft engine's total noise signature [2]. Specifically, the targeted source in this study is the so-called rotor–stator interaction tone noise generated as a result of periodic impingement of fan wakes on the outlet guide vanes (OGV). The suppression method investigated here involves incorporating swept and leaned stator vanes in the design of the OGV. As shown in Figure 1, sweep is defined as the axial displacement of the vane leading

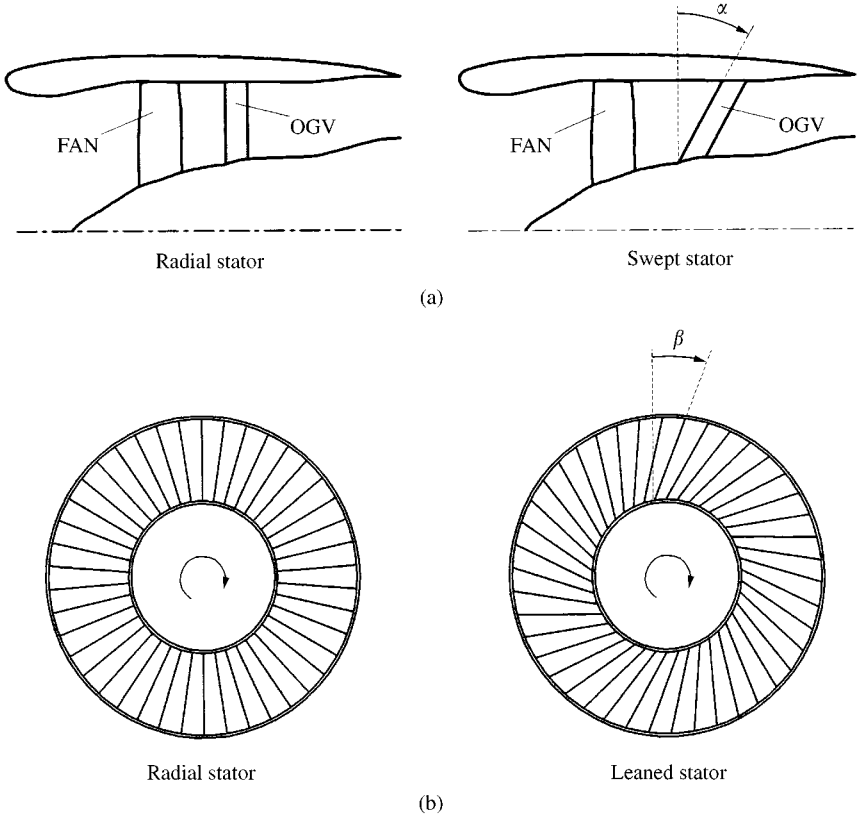

Figure 1. Geometry and definition of stator vane: (a) sweep angle and (b) lean angle. Fan rotates clockwise (view looking aft along the aft axis).

edge from its baseline radial position. Similarly, lean is the circumferential displacement of the vane leading edge from its baseline radial position.

Since the early 1970s, several theoretical and experimental studies had hinted at the potential of sweep and lean for reducing rotor–stator tone noise [3–10]. However, it was in a recent experimental study that the benefits of OGV sweep and lean for reducing fan noise were convincingly demonstrated for a representative modern low-speed fan stage [11]. The results show that, compared to a radial one, a swept and leaned OGV provides sizable reductions in the level of rotor–stator interaction tone noise over a wide range of operating conditions. Furthermore, it was also established that the swept and leaned stator was quieter even when the rotor–stator spacing for the baseline radial stator was increased. This suggests that the effectiveness of sweep and lean is not solely due to the additional viscous wake decay that is realized through the increased rotor–stator spacing for a swept and leaned OGV as compared with a radial one.

This paper documents the design procedure that was utilized to select the candidate swept and leaned OGV used in the experimental study outlined in reference [11]. The paper also includes a detailed comparative study of the predicted and measured noise benefits of the swept and leaned OGV versus the baseline radial stator as well as two other alternative low-noise configurations. A description of these alternative designs will be given later. The paper begins with an overview of the theoretical tools used in the design procedure and the details of the selection process that led to the choice of the swept and leaned OGV. In the second part of the paper, the theoretical tools used for the predicting the acoustic performance of the candidate OGV and the results of the comparative study are summarized. The comparisons serve to emphasize the advantages of the swept and leaned stator concept and, at the same time, validate the design approach and theoretical tools used in the process. A summary of conclusions drawn from this study is also included.

2. SWEEP AND LEAN DESIGN STUDY

2.1. DESIGN TOOLS

2.1.1. *Fan noise model*

The theoretical tool used in this study for selecting the candidate low-noise stator is the BBN/V072 fan noise prediction code [12–14]. It is based on an analytical model for predicting tone levels produced inside the bypass duct due to the interaction of fan wakes with the OGV. The code combines a two dimensional (2-D) strip description of the unsteady aerodynamic interaction between the rotor wakes and stator vanes with a 3-D acoustic response of an annular cascade to an incident gust. The bypass duct is assumed to be a constant-area annulus containing a uniformly moving medium. Both upstream-radiated (inlet) noise and downstream-radiated (exhaust) noise are computed by the code.

Noise computations in the BBN/V072 code are done via a two-step process. First, the unsteady surface pressure distribution induced on the vanes by the rotor

wake upwash is determined. Then, the duct noise levels resulting from the unsteady pressure distribution are calculated. Following the standard practice, noise results are expressed in terms of the fan blade passing frequency (BPF) tones. The code provides a mode-by-mode description of the inlet and exhaust noise for each tone. The mode results include cutoff ratio, sound pressure level (SPL), phase and acoustic power level.

The analysis outlined below highlights the salient features of the theoretical model in the BBN/V072 code. Details of the full derivation (in somewhat different form and notation) can be found in reference [14]. The equation governing the propagation of harmonic acoustic pressure field $p(\mathbf{x}; \omega)$ inside a duct, generated by rotor–stator interaction, is

$$p(\mathbf{x}; \omega) = \iint_{s(x_s)} \nabla G(\mathbf{x} \mid \mathbf{x}_s; \omega) \cdot \hat{n}_s f(\mathbf{x}_s; \omega) \, \mathrm{d}s(\mathbf{x}_s), \tag{1}$$

$$\mathbf{x} = (x, r, \theta), \qquad \mathbf{x}_s = (x_s, r_s, \theta_s), \tag{2}$$

where G is a 3-D frequency domain, moving medium, Green's function, f the harmonic surface pressure loading and $\hat{n}_s$ the unit surface normal. The vector $\mathbf{x}$ denotes an arbitrary field point inside the duct (with its x-component aligned with the duct axis) and vector $\mathbf{x}_s$, designates an arbitrary source location. ω, the harmonic tone frequency, is equal to $j \times \mathrm{BPF}$ ($j = 1, 2, \ldots$). S denotes all solid surfaces inside the duct (i.e., the interior of the annulus as well as the stator surface). Given an appropriate choice for G and a known distribution for f, the rotor–stator noise field can be computed by carrying out the indicated surface integration in equation (1).

While the choice of the Green's function is arbitrary, a suitable one can be computationally advantageous. The usual choice for G (with vanishing normal derivatives at the duct walls) is given by

$$G(\mathbf{x} \mid \mathbf{x}_s; \omega) = \sum_m \sum_n \frac{1}{\sqrt{(\omega/c_0)^2 - (1 - M_0^2)\kappa_{mn}^2}} \Psi_{mn}(r, \theta) \Psi_{mn}^*(r_s, \theta_s) \mathrm{e}^{\mathrm{i}\gamma_{mn}^{\pm}(x - x_s)}, \tag{3}$$

$$\Psi_{mn}(r, \theta) = [A \mathrm{J}_m(\kappa_{mn} r) + B \mathrm{Y}_m(\kappa_{mn} r)] \mathrm{e}^{\mathrm{i}m\theta}, \tag{4}$$

$$\gamma_{mn}^{\pm} = \frac{1}{1 - M_0^2} (M_0 \omega / c_0 \pm \sqrt{(\omega/c_0)^2 - (1 - M_0^2)\kappa_{mn}^2}), \tag{5}$$

where M_0 is the mean flow Mach number c_0 the nominal speed of sound of the medium inside the duct. The mean flow is assumed to be uniform and in the axial direction. The functions $\Psi_{mn}(r, \theta)$ represent normal modes of the duct indexed by m, the circumferential mode order, and n, the radial mode order. J_m and Y_m are Bessel functions of the first and second kind respectively. The parameters $\gamma_{mn}^{\pm}$ denote upstream (+) and down stream (−) axial wavenumbers of the acoutic pressure modes. The eigenvalue κ_{mn} is the root of the transcendental equation

$$\begin{vmatrix} \mathrm{J}'_m(\kappa_{mn} r_H) & \mathrm{Y}'_m(\kappa_{mn} r_H) \\ \mathrm{J}'_m(\kappa_{mn} r_T) & \mathrm{Y}'_m(\kappa_{mn} r_T) \end{vmatrix} = 0, \tag{6}$$

where r_H and r_T are the duct hub and tip radii respectively. A and B are given by either one of the following equivalent sets of values:

$$\begin{cases} A = 1, \\ B = -\dfrac{\mathrm{J}'_m(\kappa_{mn} r_H)}{\mathrm{Y}'_m(\kappa_{mn} r_H)}, \end{cases} \quad \text{or} \quad \begin{cases} A = -\dfrac{\mathrm{Y}'_m(\kappa_{mn} r_T)}{\mathrm{J}'_m(\kappa_{mn} r_T)}, \\ B = 1. \end{cases} \tag{7}$$

This choice of the Green's function reduces the integration domain in equation (1) to a subset of S that is the vane surface.

The harmonic surface pressure distribution f (at frequency ω) depends on the stator upwash (i.e., the rotor wake component normal to the vane surface). In this study the rotor wakes are modelled as frozen gusts that are convected by the mean flow. Unlike the acoustic part of the analysis, however, the mean flow (now taken to be along the chord) is assumed to be a function of the radius. The stator geometry is also simplified by assuming that vanes are infinitesimally thin twisted flat plates. With these assumptions, the chordwise distribution of the unsteady loading at each radius is related to the vane upwash velocity at that radius through the integral equation

$$w(\xi_s; r_s) = \int_{chord} K_c(\xi_s - \bar{\xi}_s; r_s) f(\bar{\xi}_s; r_s) \, \mathrm{d}\bar{\xi}_s, \tag{8}$$

where w is the upwash velocity on the vane surface, K_c the vane cascade kernel function (representing the cascade effect) and ξ_s the chordwise co-ordinate. Note that the integral equation depends only parametrically on the radial co-ordinate. The principal implication of equation (8) is that the surface loading distribution is thought of as a spanwise aggregate of 2-D chordwise distributions. This is the so-called strip approximation. With this description of f, equation (1) allows for coupling between a spanwise array of 2-D unsteady surface pressure fields and a 3-D duct acoustic field.

Returning to the analysis, a solution of equation (8) can be found if the upwash is known. Without loss of generality, the harmonic content of w (at each frequency) can be represented by

$$w(\xi_s; r_s) = A_w(r_s) \mathrm{e}^{\mathrm{i}k(r_s)\xi_s}, \tag{9}$$

where A_w is the gust harmonic amplitude and k its chordwise wavenumber which is the vector sum of the axial and tangential wavenumbers of the gust. It should be emphasized that all the variables in equations (8) and (9) represent the individual frequency content (i.e., the Fourier harmonics) of the corresponding variables in the time domain. Description of the upwash gust parameters is usually developed from empirical models of rotor steady aerodynamics or from flow measurements. More on this subject will be said later in the paper.

Since equation (8) is linear in w, it can be solved subject to a unit upwash gust. Denoting the resulting unsteady loading response as $\bar{f}$, equation (1) can be rewritten as

$$p(x) = \int_{r_H}^{r_T} \int_{chord} \nabla G \cdot \hat{n}_s A_w w(r_s) \bar{f}(\xi_s; r_s) \mathrm{e}^{\mathrm{i}\Phi(\xi_s; r_s)} \, \mathrm{d}\xi_s, \mathrm{d}r_s, \tag{10}$$

where $\Phi(\xi_s; r_s) = k\xi_s$ is the phase of the upwash. The integration over the vane surface is now explicitly stated in terms of the chordwise co-ordinate ξ_s and the radial co-ordinate r_s. Again for notational simplicity, the dependence of the acoustic pressure on frequency has been omitted.

Once the acoustic pressure is computed, the time-averaged acoustic power P generated inside the duct due to the rotor–stator interaction can be calculated. The expression for acoustic power, appropriate for a uniformly moving medium, is given by

$$P = \int_{A_D} \left[(1 + M_0^2)\langle pu_x^* \rangle + \frac{M_0}{\rho_0 c_0} \langle pp^* \rangle + \rho_0 c_0 M \langle u_x u_x^* \rangle \right] \mathrm{d}A, \tag{11}$$

where u_x is the axial component of the acoustic particle velocity, ρ_0 the medium nominal density and A_D the cross-sectional area of the duct. The symbol $\langle \cdot \rangle$ denotes time averaging over one period $2\pi/\omega$. Once the acoustic pressure p is known, u_x can be calculated via the momentum equation. Equations (10) and (11) are the principal formulae used in the BBN/V072 code for computing the tone levels generated by rotor–stator interaction.

Returning to equation (10), note the importance of the upwash phase Φ in that equation. The indicated radial integration is strongly influenced by the radial variations in Φ. If the phase varies significantly along the span (recall that k is a function of the radius), the integrand will oscillate rapidly as a function of r_s. This will cause strong cancellation between contributions from different parts of the span resulting in reduced acoustic pressure levels. Normally, the phase does not vary greatly and little cancellation occurs. However, the introduction of sweep and lean can enhance the phase variation and provide large noise reductions. The reduction can be tied directly to the vane sweep and lean as follows.

Recall the definitions of sweep and lean given in Figure 1. With these definitions, we can easily relate position of the swept and leaned vane to that of the radial vane. Expressing the relationship in terms of the chordwise co-ordinate yields

$$\xi_s' = \xi_s - (\Delta x \cos\varphi + r_s \Delta\theta_s \sin\varphi), \tag{12}$$

where ξ_s and ξ_s' denote the chordwise co-ordinate of the radial vane and swept and leaned vane respectively. The Δ's represent the displacements between corresponding points on the radial and swept and leaned vanes while φ denotes the cascade stagger angle at the current radius. Δx is the axial distance change caused by sweep and $r_s\Delta\theta_s$ the tangential (i.e., circumferential) distance change associated with lean. Note that both are functions of the radius as is the stagger angle. Using these displacement definitions, the upwash on the swept and leaned vane can be related to that for the radial vane through,

$$w(\xi_s'; r_s) = w(\xi_s; r_s) q(\Delta x) \mathrm{e}^{-\mathrm{i}k\Delta x \cos\varphi} \mathrm{e}^{-\mathrm{i}kr_s\Delta\theta_s \sin\varphi}, \tag{13}$$

where the factor $q(\Delta x)$ denotes the change in the amplitude of the baseline upwash caused by the introduction of vane sweep. This factor is needed to account for the decay of the wakes because of the increase in the rotor–stator axial spacing due to sweep. The two exponential factors represent the phase shifts introduced by vane

sweep and lean respectively. Owing to the linearity of equation (8), the loading due to the modified vane is also related to the loading for the radial vane via the same relationship as given by equation (13). Therefore, the duct acoustic pressure field for the swept and leaned vane is given by

$$p(x) = \int_{r_H}^{r_T} \int_{chord} \nabla G \cdot \hat{n}_s A_w(r_s) w(r_s) \bar{f}(\xi_s; r_s) e^{i\Phi(\xi_s; r_s)} \times \{q(\Delta x) e^{-ik\Delta x \cos\varphi} e^{-ikr_s \Delta\theta_s \sin\varphi}\} \, d\xi_s \, dr_s, \quad (14)$$

where the dependence of the various parameters on the radius is omitted for the sake of notational brevity. If sweep and lean are chosen properly, the phase terms inside the curly bracket will vary significantly as a function of the radial co-ordinate resulting in appreciable cancellations in the integral. This, in turn, will result in reduced tone levels compared with the baseline (radial) case. It should be emphasized that this cancellation effect is in addition to the reduction in the upwash amplitude denoted by $q(\Delta x)$. Consider the situation when the radial stator is moved a distance Δx downstream of its nominal location. For this configuration, the corresponding versions of the factors $q(\Delta x)$ and $\exp(-ik\Delta x \cos\varphi)$ will provide some reduction in the level of the tone, but the noise benefit will be smaller than that due to sweep and lean. This is partly because the lean effect, i.e., the factor $\exp(-ikr_s\Delta\theta_s \sin\varphi)$, will not be present for the aft-located radial stator, but also because the phasing effect due to sweep is somewhat more subtle. We shall return to this point later in section 2.3.

Returning to the description of the code, the input needed to run it includes geometric (blade and vane definitions) and fan stage steady aerodynamic performance information. An important element of the aerodynamic input information is the definition of viscous wakes of the rotor at the stator leading edge from which upwash on the vanes is determined. Wake definition in BBN/V072 is based on a set of empirical correlations that are essentially two-dimensional in nature. The correlations have an explicit dependence on the axial and tangential co-ordinates, but depend only parametrically on the radial co-ordinate. Therefore, they do not fully account for the complex nature of the flow downstream of the fan. This restriction can be avoided if wake data are used to determine the upwash. However, such a description can only be utilized if the following two requirements are met. The first is that data must be taken at the fan operating condition being considered or over a range that brackets the condition of interest. Wake data from operating conditions that are significantly different from the condition of interest cannot be used for noise predictions. The second requirement is that the wake measurement station be at or near the stator leading edge. The complicated nature of the flow behind the fan prohibits extrapolation of wake description from the axial station where measurements are taken to another axial location. In the present study, wake correlations were used since wake data were unavailable.

2.1.2. *Fan wake description*

Wake specification in the BBN/V072 code begins in the rotating (i.e., relative) reference frame. Here, for the sake of developing a mathematically tractable

representation, any radial flow that might occur is neglected. Furthermore, the flow is envisaged as a small-deficit wake profile superimposed on a parallel and locally uniform stream at each radius. Within this framework, the tangential position of the wake centerline at each radius accounts for any wake sheet tilting that might occur due to swirl. In BBN/V072, the tangential position of the wake centerline (at each radius) is determined by the relative flow angle and rotor–stator axial spacing, both of which are specified as input to the code. The change in the relative flow angle from hub to tip, therefore, represents the tilting of the wake sheet. The introduction of vane sweep and lean can enhance or diminish the wake tilting as seen by the OGV.

As was mentioned earlier, the wake profiles used in the BBN/V072 code are developed from empirical correlations. There are currently two correlation-based wake models in the code that can be used to supply wake centerline velocity deficit and half-width information. The user can choose between the correlations developed by Philbrick and Topol [15] or those developed by Majjigi and Gliebe [16].

Aside from the wake centerline velocity deficit and half-width, it is also necessary to choose a shape for the rotor wakes. The available choices in the code are a hyperbolic secant profile, a Gaussian profile and a loaded-rotor wake profile. In principle, any combination of the correlation parameters and shapes can be used to provide a complete description of wakes. In practice, however, only certain combinations produce reasonable predictions. For this study, the correlations defined in reference [15] along with the loaded-rotor wake profile were used. The chosen wake characteristics are plotted in non-dimensional form in Figure 2. The decision to use this particular combination was based on experience with similar fan stages.

Once rotor wake characteristics are specified, the resulting description is transformed to the stationary (i.e. absolute) reference frame for computing the upwash on the vanes. The upwash is then Fourier decomposed and substituted into equation (9) to start the procedure for computing the cascade unsteady pressure distribution. The resulting information is then utilized by the BBN/V072 code (equations (10) and (11) to determine the acoustic pressure and power levels for each of the propagating duct modes.

2.2. DESIGN METHODOLOGY

2.2.1. *Procedure*

In this section, we outline the design methodology that was used to identify the optimum vane sweep and lean combination. The fan stage considered for this study has 18 blades and 42 radial vanes with a design tip speed of 1000 fps. The fan tip radius is 11 in with a hub-to-tip radius ratio of 0·3.The hub-to-tip radius ratio of the stator is 0·5. The calculations were performed for takeoff (84% of the design tip speed), cutback (70% of the design tip speed) and approach (50% of the design tip speed) which are the speeds relevant to the standard noise certification procedures. Both upstream- and downstream-radiated noise contributions were considered.

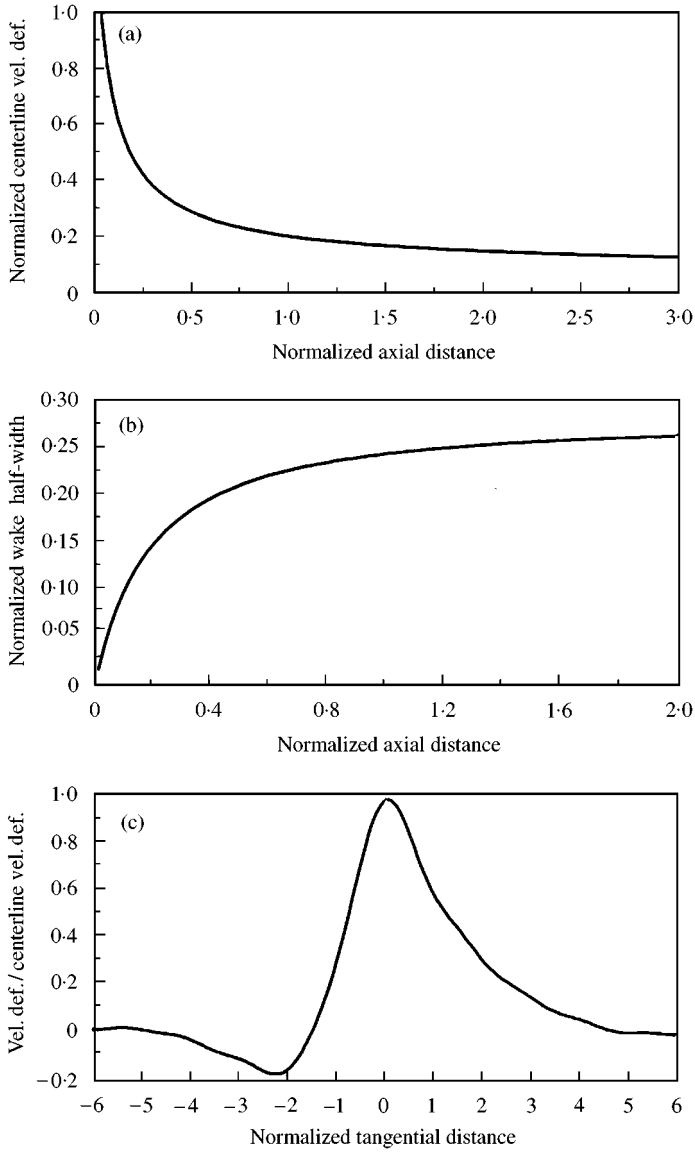

Figure 2. Rotor wake characteristics of the loaded wake model used in this study: (a) wake centreline velocity deficit, (b) wake half-width and (c) wake profile.

Pressure and power levels for all propagating modes contained within the 2BPF through 5BPF tones were computed for various combinations of sweep and lean angles. The BPF tone is cut-off for this fan stage as dictated by the Tyler–Sofrin criterion [17]. Since, on a mode-by-mode basis, the amount of information produced is enormous, it was decided that a global noise metric would be more useful in judging the benefits of sweep and lean. The metric chosen is the change in the computed tone power level from that for the radial stator. With this definition of the metric, a negative change (i.e., reduction) means acoustic benefit. The

selection process involves a case-by-case examination of a comprehensive matrix of practical sweep and lean combinations. The acoustic performance of each potential configuration is gauged by examining its calculated metric for the selected BPF harmonic at takeoff, cutback and approach. The optimum stator design is one that provides maximum overall tone noise reductions for all three operating conditions considered in this study.

We begin by defining sweep and lean via the two angles shown in Figure 1. Sweep parameter α is defined as the angle, in the meridional plane projection, between the leading edge lines of the radial and swept vanes. Positive sweep is defined as that for which vane tip is downstream of its root. Lean parameter β is defined as the angle, in the axial plane projection, between the leading edge lines of the radial and leaned vanes. Positive lean is defined in the direction opposite to rotor rotation. The matrix of the cases used for this study has sweep and lean angles ranging from -30 to 30° in increments of 5°.

2.2.2. *Results*

In Figures 3–8, the change in acoustic power (i.e., $P(\alpha, \beta) - P(0, 0)$) as a function of the sweep angle is shown for a range of lean angles. In each figure, the results for the 2BPF through 5BPF tones (subfigures (a)–(d)) are identified by open symbols. For the purposes of comparison, the reductions that are realized solely due to an equivalent axial spacing increase for the radial stator are also plotted (the isolated solid circle). The equivalent axial spacing for this aft-position radial stator, is the axial spacing between the rotor and the *tip* of the 30° swept stator. This was done to separate the noise reduction caused by the sweep-induced phase cancellation from the noise reduction caused by the increased axial spacing for the swept and leaned stators.

Figures 3 and 4 show the upstream and downstream results for the takeoff condition. Similarly, Figures 5 and 6 correspond to the cutback condition and Figures 7 and 8 to the approach condition. For the sake of clarity, the levels corresponding to only five lean angles (i.e., -30, -15, 0, 15 and 30°) are plotted. The trends for the intermediate lean angles closely follow those presented here. The results summarized in these figures show that sweep and lean have a significant impact on the predicted tone levels. Furthermore, it is clear that the operating condition, tone harmonic order and direction of noise propagation influence the effectiveness of sweep and lean. Finally, the results also show that the reductions for the aft-position radial stator are always less than the reductions for the swept and leaned stators with 30° of sweep and even modest negative leans (i.e., lean in the direction of fan rotation).

Upon a closer examination of the results in Figures 3–8, the following conclusions can be drawn. Positive sweep angles (i.e., aft sweep) always reduce the tone levels while negative sweep angles increase them. The influence of lean, on the other hand, is more subtle. In most cases, for a given (positive) sweep, negative lean angles enhance the benefits of sweep by causing additional noise reductions. In contrast, positive lean angles tend to diminish, or even offset, the benefits of sweep (see Figure 4(d), for example). Finally, a comparison of the tone reductions for the

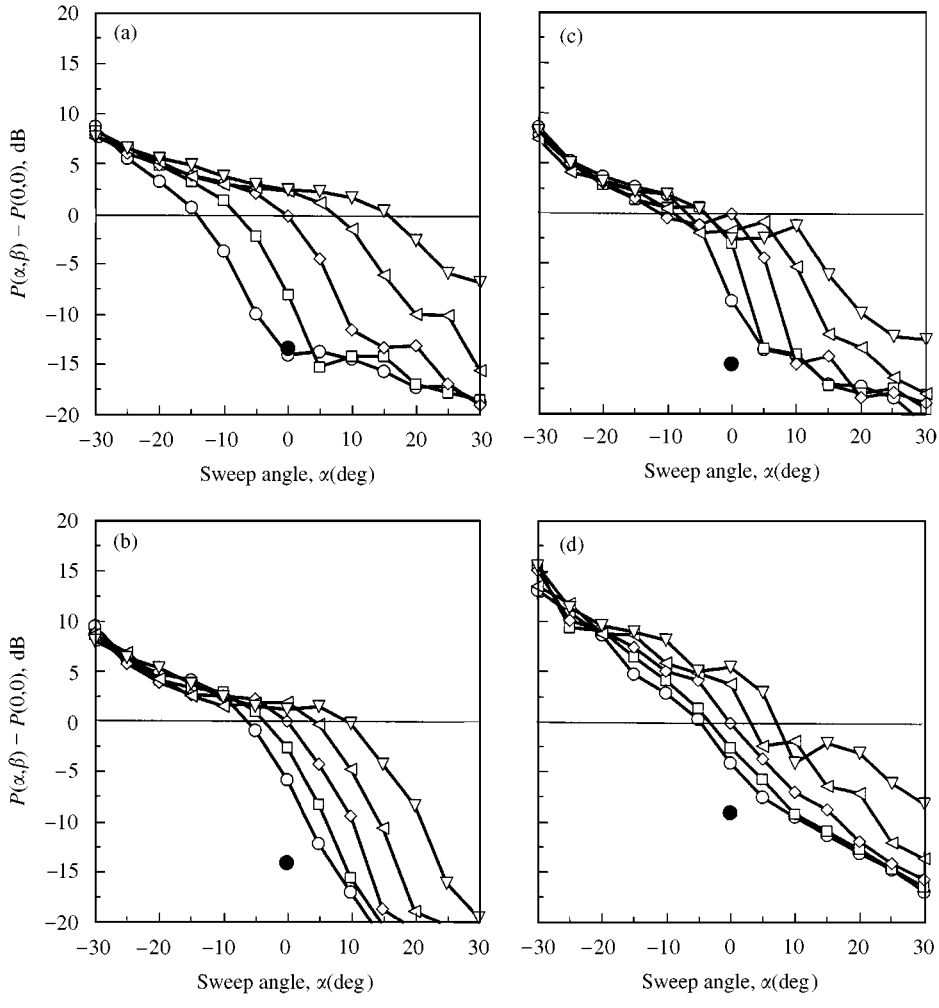

Figure 3. Influence of vane sweep and lean on the predicted rotor–stator interaction tone noise. Upstream tone power at takeoff condition: (a) 2BPF, (b) 3BPF (c) 4BPF and (d) 5BPF levels; ○, $-30°$ lean; □, $-15°$ lean; ◇, 0° lean; ◁, 15° lean; ▽, 30° lean; ●, radial stator in the aft position.

30° swept stator (denoted by ◇) and the radial stator in the aft position (denoted by ●) reveals that, with few exceptions, the sweep alone produces more reductions than mere axial spacing increase. (Recall the discussion following equation (14)).

2.3. NOISE REDUCTION MECHANISM

As was stated earlier, the predicted behavior with sweep and lean can be explained in terms of their influence on the harmonic phase of the upwash along the vane span. Recall that, according to equation (14), the strength of the noise source is strongly influenced by the spanwise phase of the upwash. Significant upwash

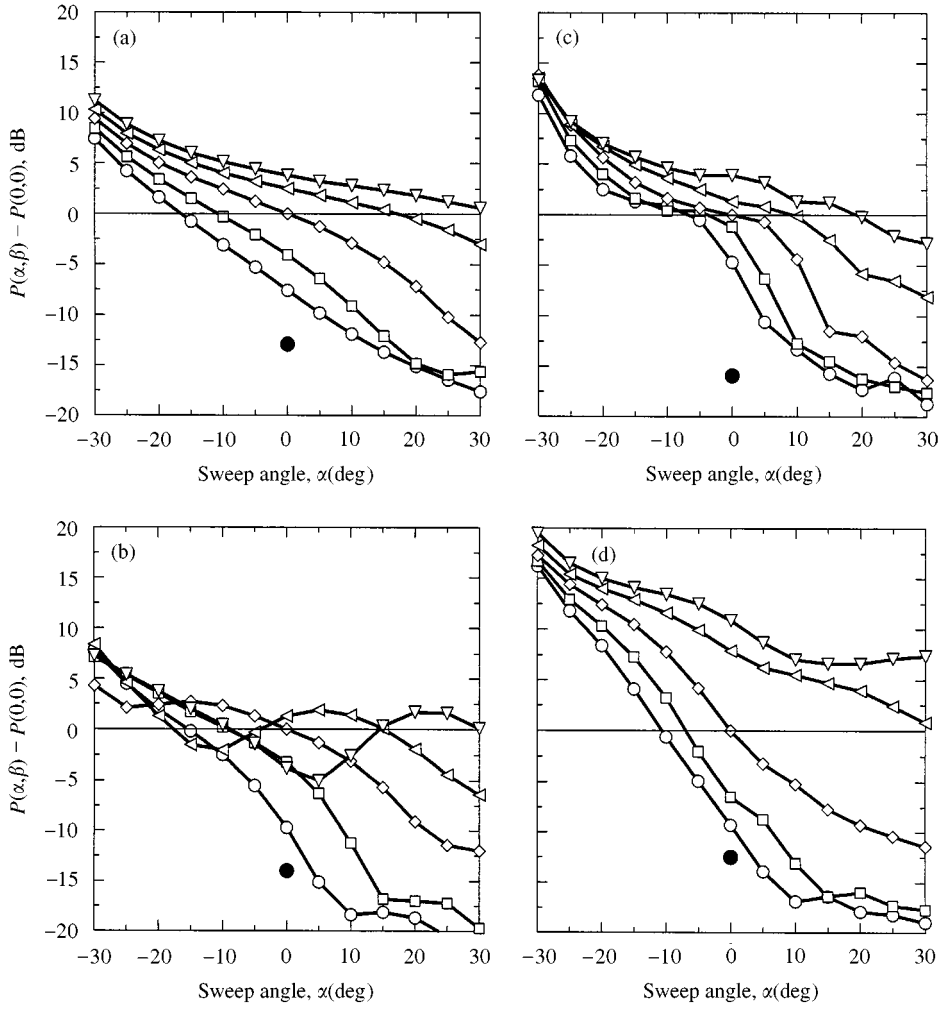

Figure 4. Influence of vane sweep and lean on the predicted rotor–stator interaction tone noise. Downstream tone power at takeoff condition: (a) 2BPF, (b) 3BPF (c) 4BPF and (d) 5BPF levels; ○, −30° lean; □, −15° lean; ◇, 0° lean; ◁, 15° lean; ▽, 30° lean; ●, radial stator in the aft position.

spanwise phase variation causes noise cancellation between contributions from different locations along the vane span resulting in weaker interaction tones. For the most part, variation in the spanwise phase of the upwash is controlled by the number of individual rotor wakes that intersect a given vane. This number is determined, primarily, by the kinematics of the rotor wakes in relation to the stator vanes. Swirl variation from hub to tip introduces a tangential shift between the circumferential positions of the wakes along the span. The shift increases with downstream distance causing the wake sheet of a single rotor blade to intersect more than one stator vane at the time. Stated in equivalent terms, wake sheets from more than one rotor blade intersect a single vane. A schematic description of this effect is depicted in Figure 9.

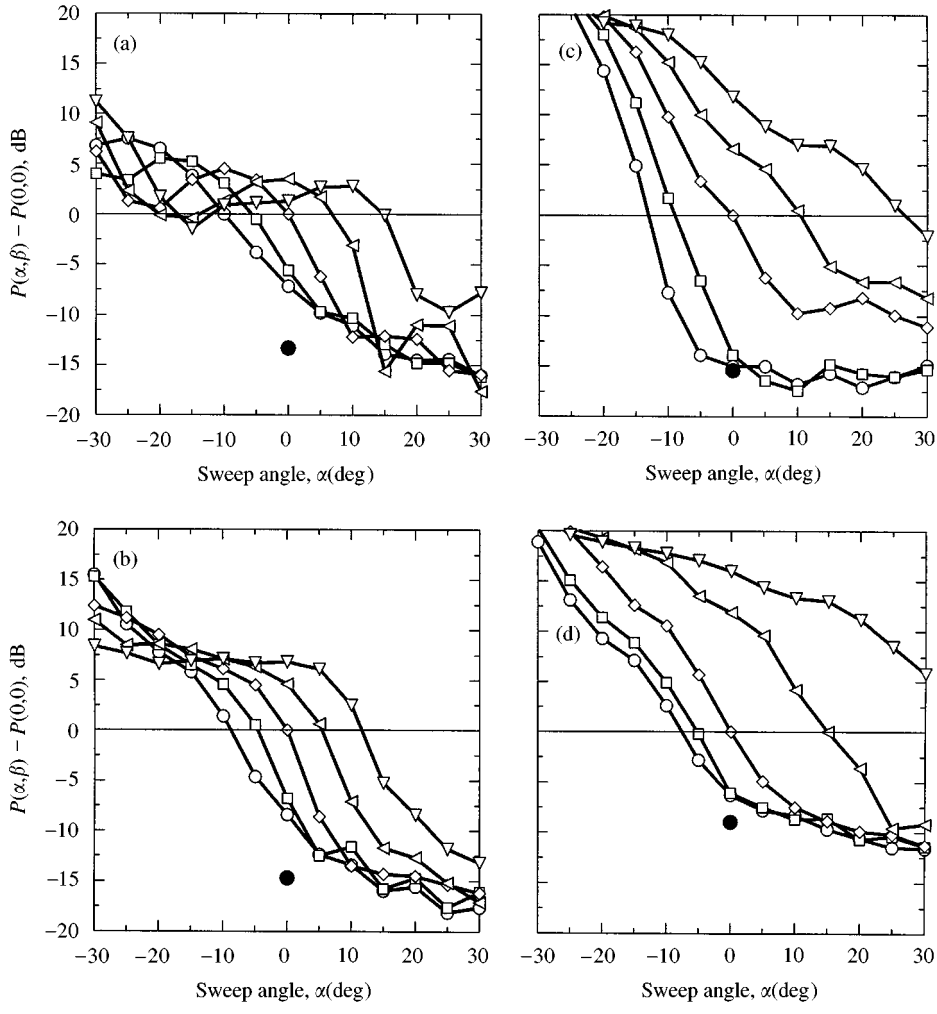

Figure 5. Influence of vane sweep and lean on the predicted rotor–stator interaction tone noise. Upstream tone power at cutback condition: (a) 2BPF, (b) 3BPF (c) 4BPF and (d) 5BPF levels; ○, −30° lean; □, −15° lean; ◇, 0° lean; ◁, 15° lean; ▽, 30° lean; ●, radial stator in the aft position.

For a typical fan stage, there usually occur a few intersections per vane. However, for a fixed number of blades and vanes, the introduction of vane sweep and/or lean, changes the number of intersections per vane. The change occurs because sweep and lean alter the kinematic relationship between the wakes and vanes. Figure 10 shows the crucial influence of sweep and lean in determining the number of intersections for three choices of sweep and lean. View is looking downstream along the fan axis. Sketch (a) in this figure depicts the baseline kinematic picture for a radial stator. Sketches (b) and (c) show the change in the relative kinematics for a "beneficial" combination of sweep and lean and a "detrimental" one respectively. A correct choice of sweep and lean (b) results in additional intersections compared with the radial case, while an incorrect choice (c) reduces the number of

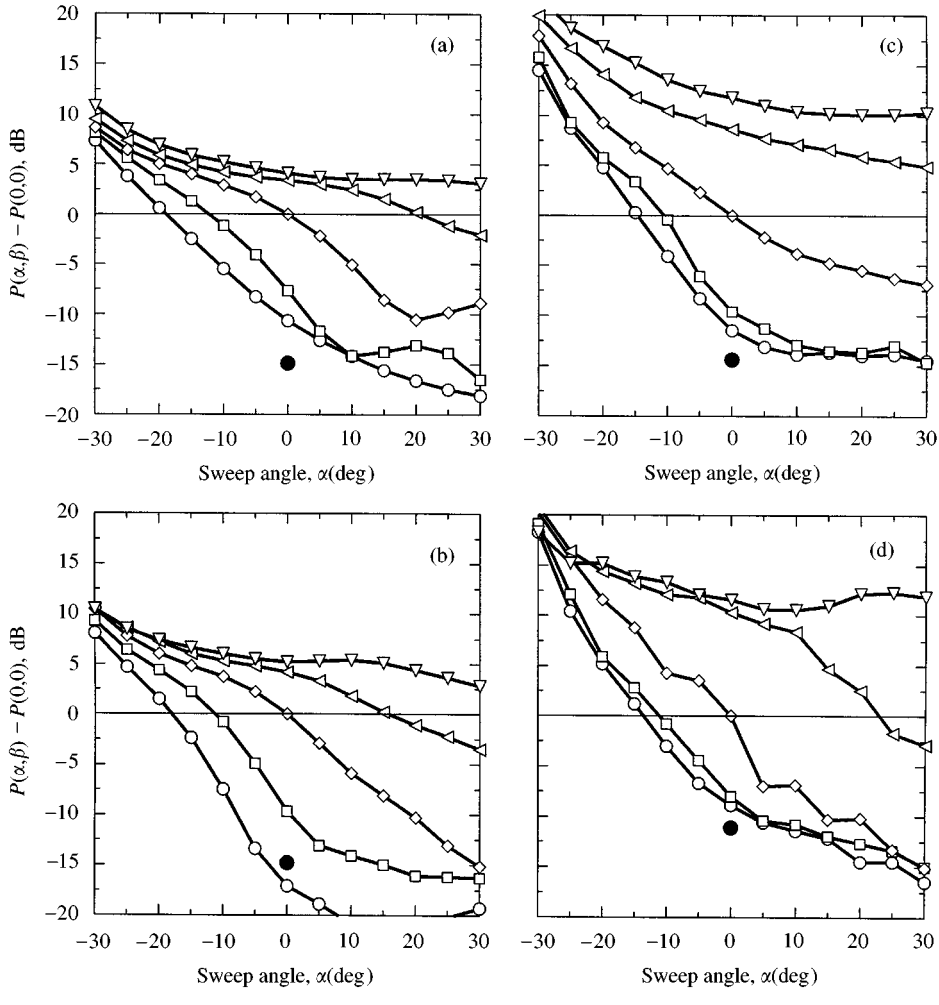

Figure 6. Influence of vane sweep and lean on the predicted rotor–stator interaction tone noise. Downstream tone power at cutback condition: (a) 2BPF, (b) 3BPF (c) 4BPF and (d) 5BPF levels; ○, $-30°$ lean; □, $-15°$ lean; ◇, 0° lean; ◁, 15° lean; ▽, 30° lean; ●, radial stator in the aft position.

intersections. A beneficial combination increases the streamwise distance between the rotor and the stator allowing more wake tilting to occur. Conversely, an incorrect choice reduces the rotor–stator distance resulting in less tilting before the wake impingement. Therefore, the most important conclusion to be drawn from Figure 10 is that a correct combination of sweep and lean is crucial if maximum noise benefits are to be realized. In fact, an incorrect combination can increase the noise levels. Consider, for example, the predicted noise level changes in the inlet at 2BPF for the takeoff condition (Figure 3(a)). For this condition, compare the beneficial combination of sweep and lean ($\alpha = 30°$, $\beta = -30°$) for which noise is reduced and the detrimental combination ($\alpha = -30°$, $\beta = 30°$) for which noise is increased.

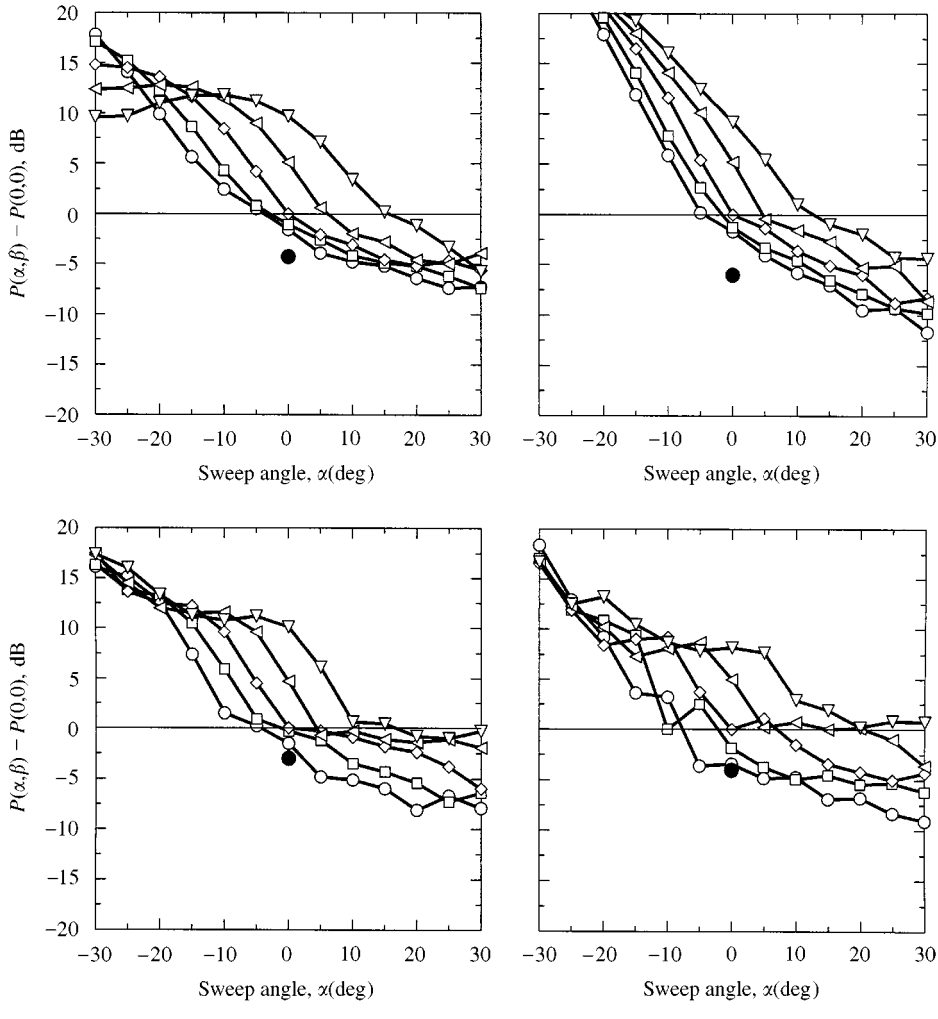

Figure 7. Influence of vane sweep and lean on the predicted rotor–stator interaction tone noise. Upstream tone power at approach condition: (a) 2BPF, (b) 3BPF (c) 4BPF and (d) 5BPF levels; ○, $-30°$ lean; □, $-15°$ lean; ◇, 0° lean; ◁, 15° lean; ▽, 30° lean; ●, radial stator in the aft position.

In Figure 11, plots of the spanwise harmonic phase variation of the upwash for these three sweep and lean configurations are shown. Note that, compared with the radial stator, the beneficial configuration (b) has significantly more spanwise phase variation than the detrimental one (c). In fact, the latter has less variation compared with the radial stator (a). It is instructive to compare these phase plots with the kinematic description shown in Figure 10. Compared with the radial stator, the combination ($\alpha = 30°$, $\beta = -30°$) allows for more wake–vane intersections and, therefore, more spanwise phase variation. Conversely, for the combination ($\alpha = -30°$, $\beta = 30°$) fewer intersections lead to less phase variation.

Now let us examine the impact of the upwash phase variation on the predicted vane unsteady surface pressure distribution. In Figure 12, phase contours of the

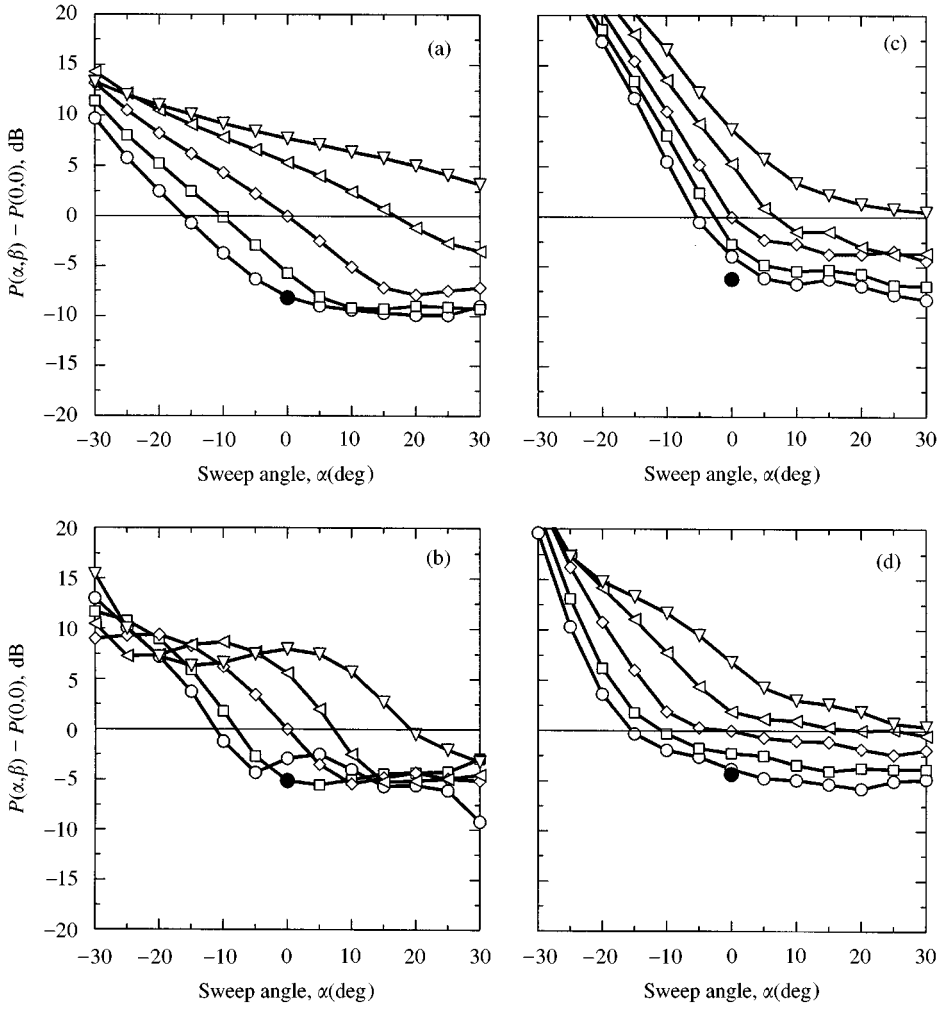

Figure 8. Influence of vane sweep and lean on the predicted rotor–stator interaction tone noise. Downstream tone power at approach condition: (a) 2BPF, (b) 3BPF (c) 4BPF and (d) 5BPF levels; ○, $-30°$ lean; □, $-15°$ lean; ◇, 0° lean; ◁, 15° lean; ▽, 30° lean; ●, radial stator in the aft position.

unsteady surface pressure corresponding to the three sweep and lean combinations of Figure 11 are shown. Compared with the radial stator (a), the correct choice of sweep and lean (b) produces significantly more variation in the phase of surface pressure. In contrast, the incorrect choice (c) actually reduces the phase variation. Recall that, the tone level is related to the surface integral of the vane unsteady pressure (see equation (10)). Therefore, the more phase variation there is in the unsteady pressure, the more cancellations will occur in the integral resulting in a weaker tone as seen in Figure 3 for the combination ($\alpha = 30°$, $\beta = -30°$). On the other hand, if there is less phase variation, there will be less cancellation leading to higher tone levels as seen for the combination ($\alpha = -30°$, $\beta = 30°$).

The results shown in Figures 10–12 corroborate the argument regarding the role of sweep and lean in changing the tilt of the rotor wakes relative to the stator vanes.

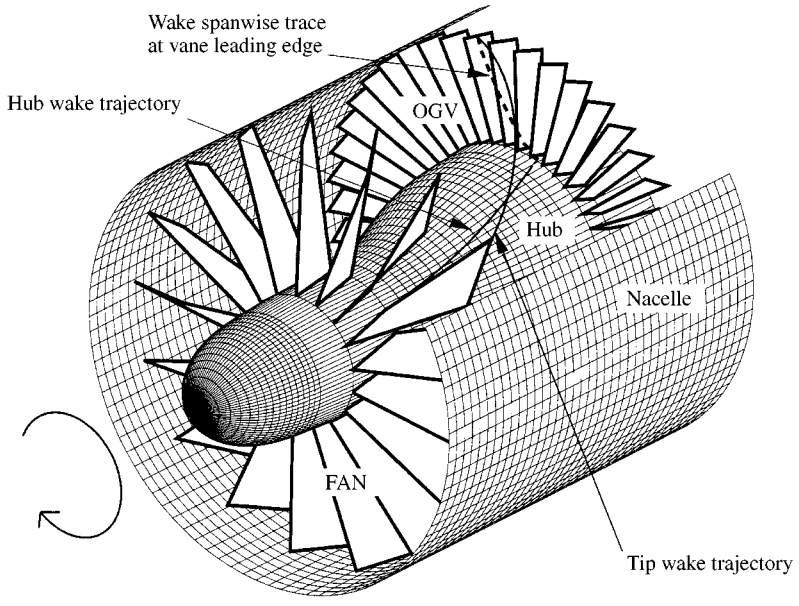

Figure 9. Schematic depiction of the kinematic relationship between rotor wakes and stator vanes. Wake tilting is caused by swirl variation from hub to tip. Situation for a radial stator is shown.

They also clearly demonstrate the importance of the proper choice of sweep and lean combination. Of course, as was stated earlier, the realized sweep and/or lean benefits vary with fan tip speed and tone harmonic order. In general, the predicted noise reductions tend to be more significant at higher tip speeds and for higher tone harmonics. Both of these observations are consistent with the kinematic argument. The tip speed trend is justifiable because over the same streamwise distance the higher fan tip speed at takeoff produces more wake tilting than does the lower tip speed at approach. Similarly, the benefits are larger for higher tone harmonics, because upwash harmonic phase variation is directly proportional to the harmonic order. So, for example, if there are three sign changes in the spanwise phase of the upwash at 2BPF there will be twice as many at 4BPF and so on.

2.4. SELECTED OGV DESIGN

The theoretical results presented above indicate that, to reduce rotor–stator interaction tone noise, stator vanes should have aft sweep and should be leaned in the direction of fan rotation. Furthermore, they also suggest that there are more acoustic benefits for larger sweep and lean angles. Therefore, it was decided to implement the largest sweep and lean angles that were structurally and aerodynamically feasible. These requirements resulted in a swept and leaned vane design having 30° of aft sweep (i.e., $\alpha = 30°$) and 30° of lean in the direction of fan rotation (i.e., $\beta = -30°$). To separate the benefits of sweep and lean, a swept-only

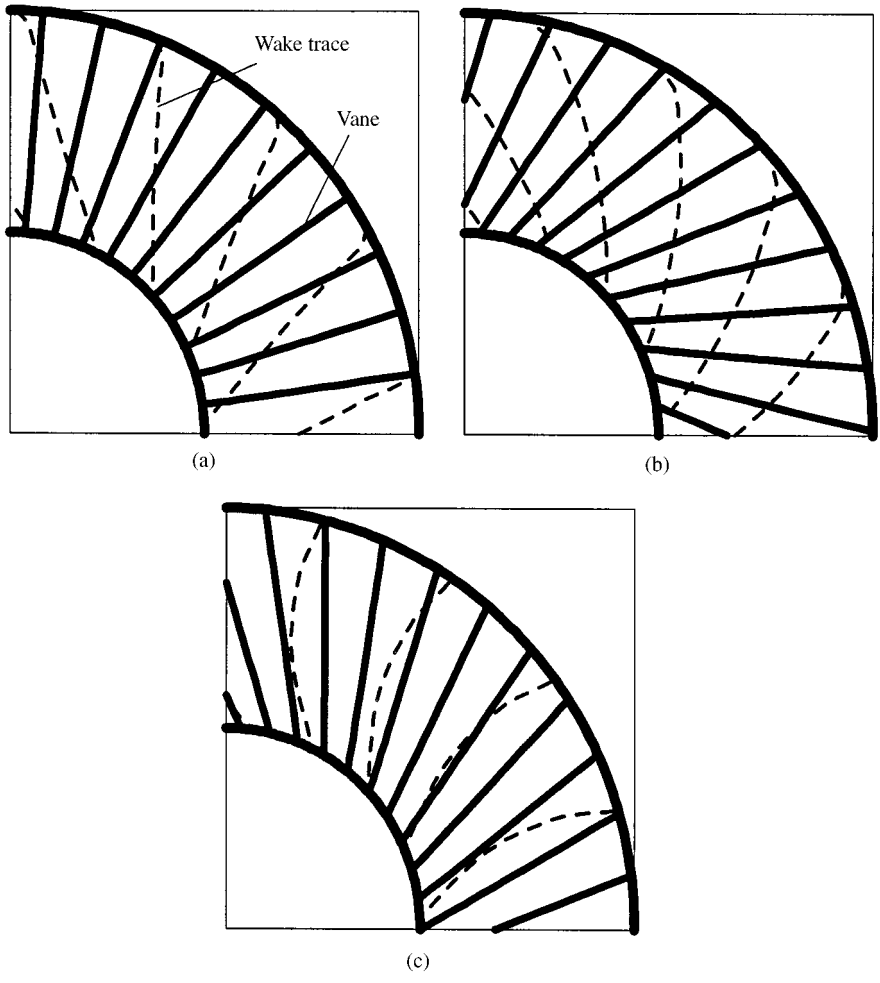

Figure 10. Wake centerline traces (dashed lines) at the stator LE (solid lines): (a) radial stator, $\alpha = 0^\circ$, $\beta = 0^\circ$; (b) a beneficial combination of vane sweep and lean $\alpha = 30^\circ$, $\beta = -30^\circ$; (c) a detrimental combination $\alpha = -30^\circ$, $\beta = 30^\circ$. Fan rotates clockwise (view looking aft along the fan axis). One-quarter of annulus is shown.

stator (i.e., $\alpha = 30^\circ$, $\beta = 0^\circ$) was also built. Recall that the aft-position radial stator is louder (i.e., produces less noise reductions) compared with this combination of stator sweep and lean at any speed. To verify the validity of this prediction, the radial stator was also tested in aft position. Photographs of the fan stage assembly with the swept-only and swept and leaned stators are shown in Figure 13.

The Allison Engine Company, under contract to NASA Glenn Research Center, built the fan stage and all of the tested stator configurations [18]. The selected stators were tested in the NASA Glenn $9' \times 15'$ Acoustic Wind Tunnel where detailed farfield noise measurements were obtained at several fan operating conditions including those reported in this paper. A detailed description of the

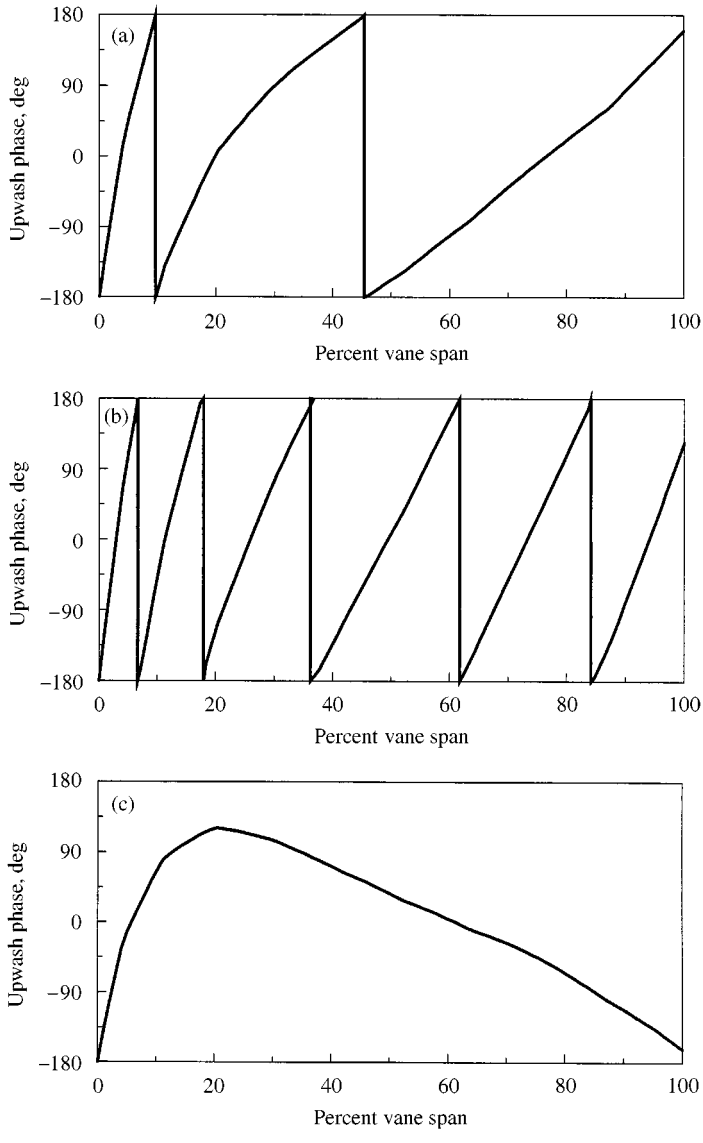

Figure 11. Spanwise phase of the 2BPF harmonic component of the upwash at the takeoff condition: (a) radial stator, (b) a beneficial combination of vane sweep and lean and (c) a detrimental combination; α and β as in Figure 10.

experimental set-up, the noise measurement technique and the measured sideline directivities are presented in reference [11]. The test data unequivocally show that, compared to the radial OGV, the swept and leaned OGV is quieter at all tested conditions. The swept-only stator also shows sizeable acoustic benefits. Later in this paper, detailed comparisons between the measured and predicted sideline directivities of the radial, swept-only and swept and leaned stators will be presented.

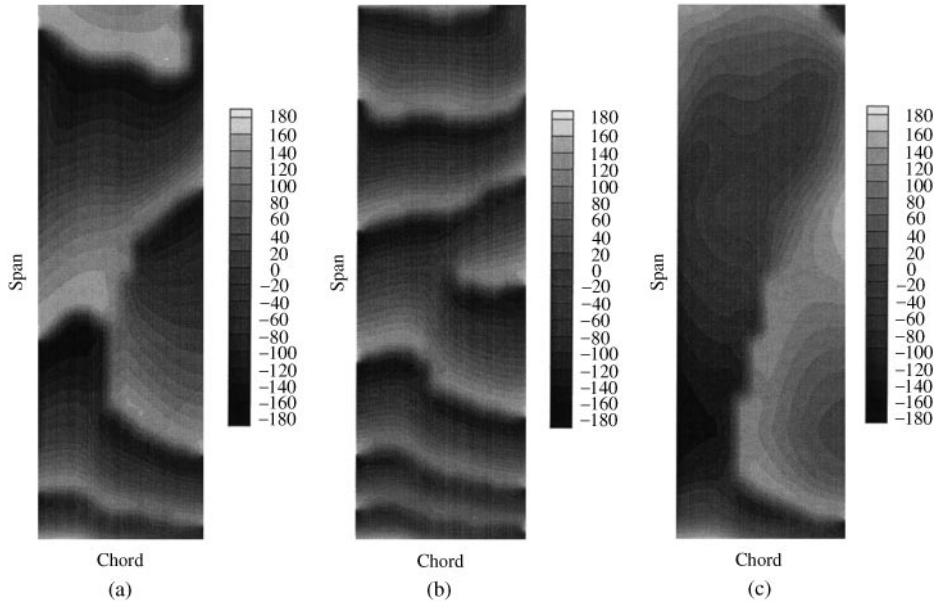

Figure 12. Theoretically predicted phase contours of vane unsteady surface pressure: (a) radial stator, (b) a beneficial combination of vane sweep and lean and (c) a detrimental combination α and β as in Figure 10. Vane planform is mapped to a rectangle to facilitate comparisons.

3. ANALYSIS OF THE SWEPT AND LEANED STATOR

3.1. ANALYSIS TOOLS

The predicted sideline directivities are calculated using the Eversman radiation codes designed to predict the farfield tone noise radiation from inlet and exhaust sections of a fan bypass duct [19, 20]. As shown in Figure 14, the inlet and exhaust codes compute the radiation fields in the forward and aft arcs respectively. In each case, the arc covers a region extending from the fan axis to a location well past the 90° position. In the overlap region, the linear nature of the wave equation permits the addition of the two solutions (with the phase taken into account) to obtain the complete sideline directivity.

Both of these codes are based on a frequency-domain, finite element formulation of the problem of acoustic radiation from termination of an axisymmetric duct. They solve for the acoustic field (both inside and outside of the duct) once the internal geometry of the duct and the in-duct pressure levels are specified. The specification of the internal acoustic field is in terms of amplitudes of the cut-on duct modes at the internal boundary of the computational domain. The mode input can be supplied from in-duct measurements or from predictions (from the BBN/V072 code, for example). The duct internal and external flowfields are assumed to be irrotational and are calculated as part of the solution. The computational domain for each code is the region that starts at the input plane inside the duct and extends outside of the duct between the fan axis and a suitably

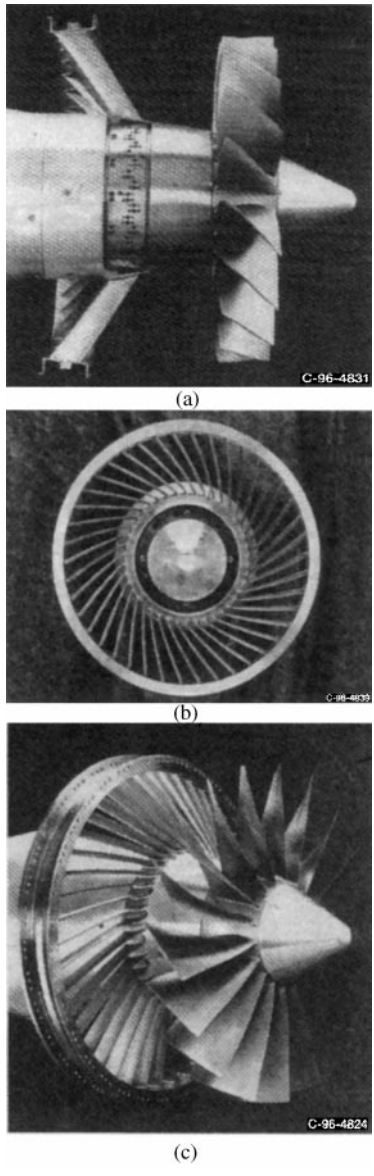

Figure 13. Photographs of the partially assembled fan stages: (a) is the side view of the swept stator; (b) and (c) are different views of the swept and leaned stator.

chosen "baffle" (see Figure 14). Care is taken to keep the baffle position far away from the source region so that its influence on the solution is negligible [21]. Both lined (i.e., absorbent) and unlined (i.e., hard) boundary conditions can be specified on the duct walls. On the farfield boundaries (i.e., arcs) and on the baffle, a Sommerfeld radiation condition is specified.

For the exhaust problem, the presence of the jet shear layer requires implementation of additional constraints in the calculations. For the mean flow,

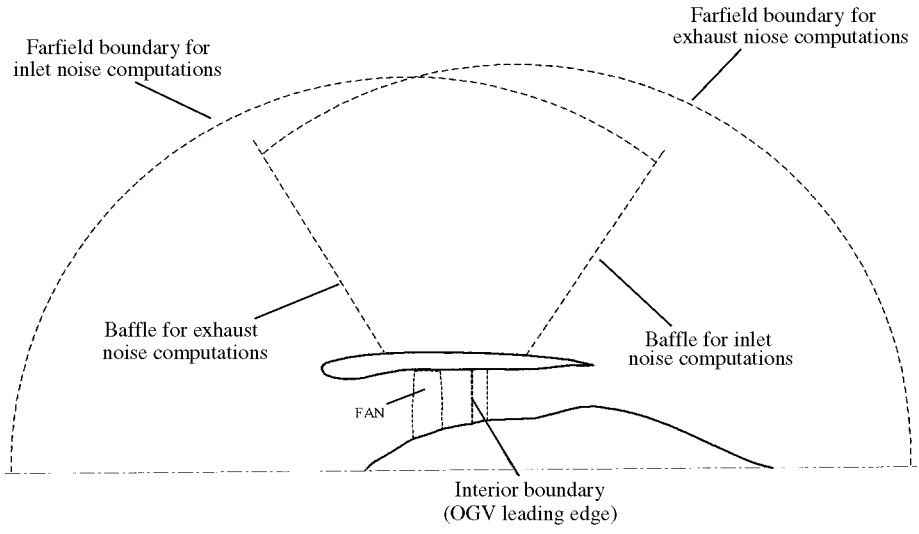

Figure 14. Computational domains for inlet and exhaust radiation computations.

since the dynamics of the shear layer is highly complicated, a simplified condition is used. The shear layer is modelled as though the bypass duct extends some distance downstream of the exist plane. Therefore, in the extended region, the flow is composed of two parts, an inner flow and an outer flow, and the velocity potential is discontinuous across the layer separating them. But, beyond this extended region, the velocity potential is assumed to be continuous and the internal and external flows are permitted to mix on a potential flow basis. The extent of the "fictitious duct" is chosen so as to provide realistic acoustic wave diffraction effects across the shear layer while at the same time minimizing the influence of the artificial mixing on the acoustic field (see reference [20]). This treatment of the shear layer is found to work reasonably well for the moderate flow Mach numbers considered in this paper. For the acoustic calculations, the presence of the shear layer necessitates the specification of two continuity conditions along the interface. These are the continuity of acoustic pressure across the shear layer and the continuity of displacement of the interface itself. The latter is a kinematic condition arising from the assumption that the interface acts as an impermeable membrane across which acoustic perturbations are transmitted by virtue of its motion.

The geometry and the steady flow field are assumed to be axially symmetric and the mean flow is taken to be inviscid and irrotational. The acoustic field equations are obtained by considering small perturbations superimposed on the mean flow. The noise source is decomposed into its circumferential modal content allowing for a two-dimensional representation of the acoustic field in an (x, r) plane through the axis of symmetry. Acoustic perturbations are represented as harmonic disturbances and are Fourier decomposed in the circumferential co-ordinate. After some manipulations of the governing equations in linearized form, the formulation

leads to

$$\iiint_V \{\nabla W \cdot (\rho_0 \nabla\phi + \rho \nabla\phi_0) - \mathrm{i}\eta W\rho\}\,\mathrm{d}V = \iint_S W(\rho_0 \nabla\phi + \rho \nabla\phi_0)\cdot \hat{n}_s\,\mathrm{d}S, \quad (15)$$

where ϕ is the acoustic velocity potential, ρ the acoustic density, V the computational volume and S all solid surfaces. The corresponding mean flow quantities are identified by the subscript "0". It should be noted that, here, the mean flow quantities are not uniform but depend on the axial and radial co-ordinates. The non-dimensional frequency is defined as $\eta = \omega R/c_\infty$ where ω is the dimensional source frequency, R is a reference length (generally, taken to be the duct radius at the source plane) and c_∞ the farfield (ambient) speed of sound. The acoustic velocity potential is non-dimensionalized by the quantity $c_\infty R$ and the acoustic pressure by $\rho_\infty c_\infty^2$ where ρ_∞ is the density in the far field. Time is scaled by R/c_∞ and M_∞ denotes the Mach number in the far field representing the forward flight effect.

The weighting functions are taken as $W(x, r, \theta) = \bar{W}(x, r)\mathrm{e}^{\mathrm{i}m\theta}$. Circumferential modes, denoted by $\mathrm{e}^{\mathrm{i}m\theta}$, represent the decomposition of the solution in θ via a Fourier series where m is the circumferential mode number. The unit normal $\hat{n}_s$ is out of the domain at the surface being considered. The linearized momentum equation

$$\rho = -(\rho_0/c_0^2)(\mathrm{i}\eta\phi + \nabla\phi_0 \cdot \nabla\phi) \quad (16)$$

is used for substituting for ρ in equation (15). The linearized equation of state is $p = \rho c_0^2$. The weighted residual formulation for the steady flow is

$$\iiint_V \nabla W \cdot (\rho_0 \nabla\phi_0)\,\mathrm{d}V = \iint_S W(\rho_0 \nabla\phi_0)\cdot \hat{n}_s\,\mathrm{d}S, \quad (17)$$

where γ is the ratio of specific heats. The steady flow momentum is written in terms of steady flow density via

$$\rho_0 = \left[1 - \frac{(\gamma - 1)}{2}(\nabla\phi_0 \cdot \nabla\phi_0 - M_\infty^2)\right]^{1/(\gamma-1)}. \quad (18)$$

The acoustic pressure is the physical quantity that is measured for comparison between the theory and experiment. The pressure is specified at the input plane using the modal decomposition

$$p_{mn}(r) = A_{mn}[J_m(\kappa_{mn} r) + Q_{mn} Y_m(\kappa_{mn} r)], \quad (19)$$

where κ_{mn} is the eigenvalue of the duct corresponding to the mode indexed by (m, n) and $Q_{mn} = -J'_m(\kappa_{mn} r_H)/Y'_m(\kappa_{mn} r_H)$. Both of these parameters are functions of the hub-to-tip radius ratio. The radial co-ordinate r is normalized by the source plane radius R. The acoustic pressure is related to the acoustic velocity potential via the momentum equation

$$p_{mn} = -\mathrm{i}\rho_0(\eta - \gamma_{mn} U)\phi, \quad (20)$$

where U is the mass-averaged axial velocity at the source plane.

Recent applications of this type of an approach to the prediction of farfield fan noise may be found in references [22–25]. In the present work, using mode predictions from the BBN/V072 code as input for the radiation codes, sideline directivities were computed for four stator configurations of interest. Recall that, these include the radial stator in its nominal forward position, radial stator in the aft position, swept-only stator and swept and leaned stator. The computed results were then compared with the corresponding measured data. The comparisons were carried out for the 2BPF tone at the approach, cutback and takeoff conditions and for the 3BPF tone at the approach condition only. The sideline, where noise data were taken, is 88 in away from the fan axis. The tunnel Mach number is 0.1 chosen to guarantee that the background tunnel noise level was well below the noise from the fan model [26]. It should be emphasized that all of the theoretical results will be shown without any adjustments or shifts in their levels.

3.2. SIDELINE DIRECTIVITIES (2BPF RESULTS)

3.2.1. *Radial stator*

We begin the data-theory comparisons with the radial stator in the forward position whose results are shown in Figure 15. The figure shows plots of 2BPF tone SPL as a function of the emission angle for each speed considered in this report. The symbols represent the measurements and the solid curves the predictions. The thin line connecting the data points is drawn to aid in discerning the pattern of the measured directivities. To help analyze the trends, the measured broadband noise level at 2BPF is also shown (dashed line). The SPL range for each graph is chosen to provide the best overall representation of the results but the increment is kept the same for all graphs to allow for easy comparisons.

The radial OGV results show that there is generally a good agreement between the predicted and measured directivities for the approach and cutback conditions, but that the agreement is only marginal for the takeoff condition. In particular, at approach the predicted peak SPL and peak radiation angles for both inlet and exhaust are well predicted. In fact, over the entire range of emission angles, the predicted directivity is close to the measured one. On the other hand, the data-theory agreement for takeoff is rather poor. For this speed, there are significant overpredictions in both the inlet and exhaust portions of the directivity. For the cutback condition, there is fair agreement in the inlet but significant overprediction in the exhaust. It should be noted that where the measured tone is very close to the broadband level, the tone level could not be reliably measured. Similarly, the sharp dips in the predicted directivities are somewhat unrealistic and should be "clipped" at the broadband level. It is these clipped predictions that should be compared with the measured tone levels. With that in mind, the data-theory comparisons are improved, particularly, for the approach condition. Overall, given the simplifications made in modelling the noise source and, to a lesser extent, those employed in the radiation predictions, the overall data-theory agreement is very encouraging.

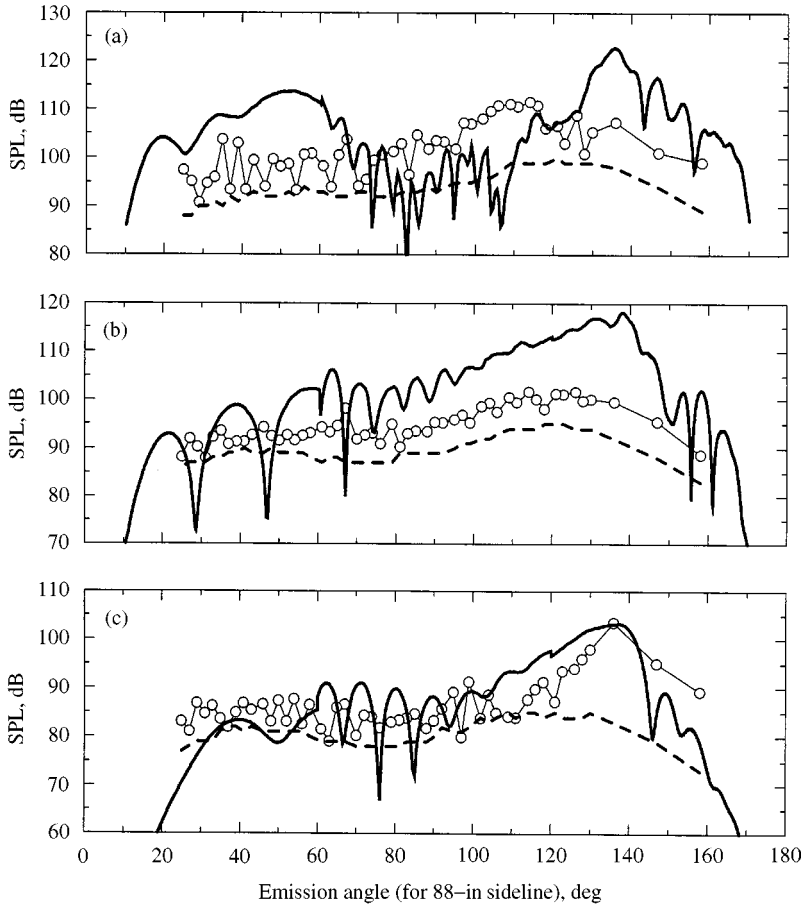

Figure 15. Comparison of measured (symbols) and predicted (solid line) 2BPF tone farfield directivities for the nominal radial stator. Measured broadband noise level (dashed line) at 2BPF tone is also shown. (a) Shows the takeoff levels, (b) the cutback levels and (c) the approach levels.

3.2.2. *Swept-only stator*

The results for the swept-only stator are summarized in Figure 16. For this configuration, the absolute 2BPF levels are significantly lower than those for the radial stator and so they are closer to the broadband noise levels. Overall, the data-theory agreement is remarkably good. Here the trends, as well as the levels, are well predicted for all three speeds. There are, nonetheless, local discrepancies especially for the cutback and takeoff conditions for which the theory overpredicts the measured exhaust SPL at large emission angles. Note that, both the measured and predicted levels for the swept-only stator show sizable reductions compared to the levels for the radial stator levels as discussed below.

Predicted and measured 2BPF tone reductions due to sweep (i.e., swept-only OGV levels minus radial OGV levels) are shown in Figure 17. Note that with this

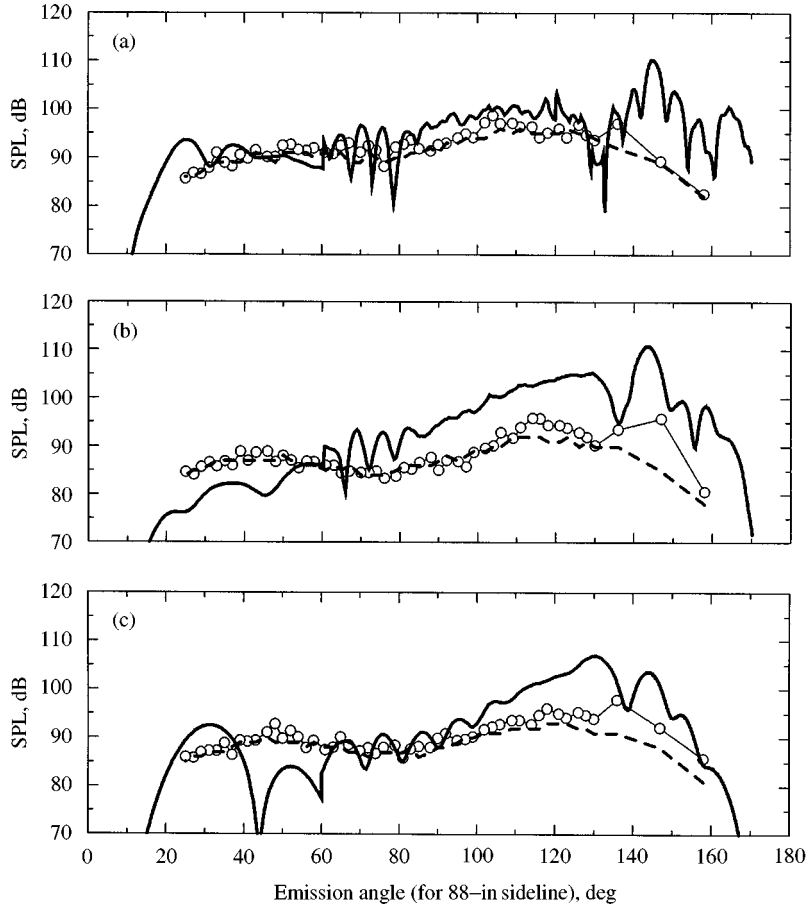

Figure 16. Comparison of measured (symbols) and predicted (solid line) 2BPF tone farfield directivities for the swept-only stator. Measured broadband noise level (dashed line) at 2BPF tone is also shown. (a) Shows the takeoff levels, (b) the cutback levels and (c) the approach levels.

definition, the 0-dB line represents the level for the radial stator. The symbols now indicate the measured tone reductions and the solid lines represent broadband-corrected predictions calculated using the clipped predictions that were discussed earlier. The measured benefits, while not uniform, are generally centered on the 5-dB level for the approach condition, around the 7·5-dB level for the cutback condition and around the 10-dB level for the takeoff condition. As for the predictions, at approach and cutback, the bulk of the noise reductions fall in the 5–10-dB range. For takeoff, the predicted reductions are somewhat larger and more erratic. This is, of course, the result of the fact that the predicted radial stator levels do not agree well with the data even though the levels for the swept-only stator do. Nevertheless, the general trend of reductions with the fan tip speed is reasonably well predicted in the sense that the reductions are higher at takeoff compared to those for approach and cutback.

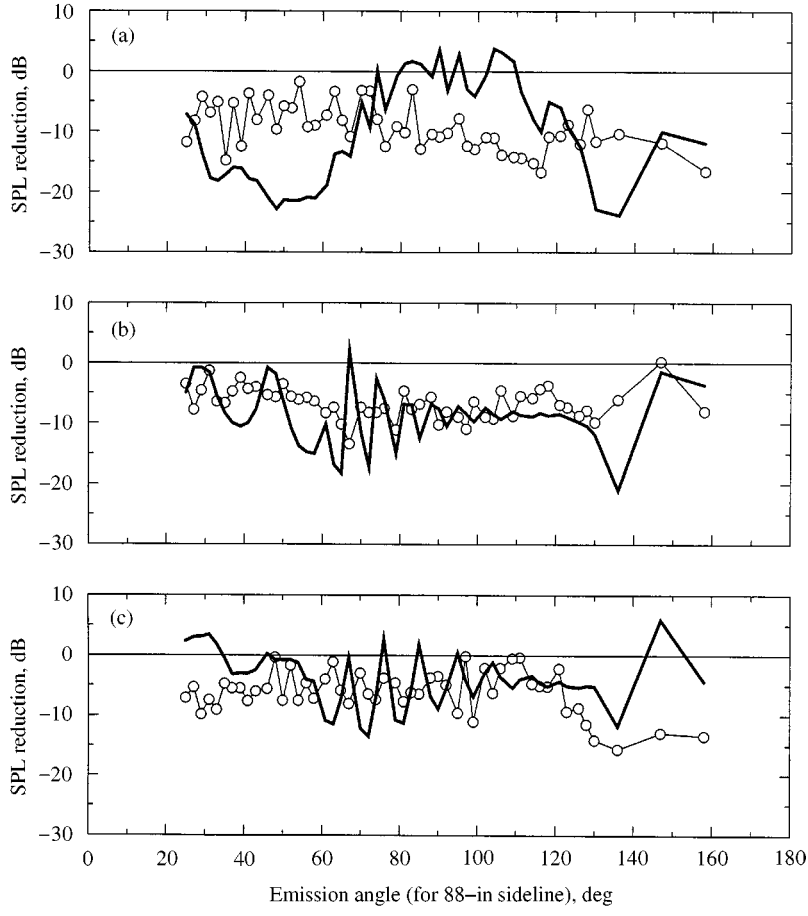

Figure 17. Comparison of measured (symbols) and broadband-corrected predicted (solid line) 2BPF tone reductions in the far field due to sweep. Radial stator level is the baseline (i.e., 0 dB). (a) Shows the takeoff levels, (b) the cutback levels and (c) the approach levels.

3.2.3. *Swept and leaned stator*

Next, the comparisons for the swept and leaned stator (i.e., $\alpha = 30^\circ$, $\beta = -30^\circ$) are shown in Figure 18. Note that for this configuration, the absolute levels for the 2BPF tone are essentially at the broadband level. This suggests that the sharp oscillations in the predicted levels should be ignored when comparing the theoretical and experimental results. With that in mind, the general agreement between the data and theory is very good for this configuration with the predicted SPL being very close to the measured one for all three speeds.

Figure 19 shows the 2BPF tone SPL reductions when the radial stator levels are used as the baseline. The broadband-corrected theoretical reductions compare quite well with the measured reductions for approach and cutback, but the comparison is poor at takeoff. The agreement for the takeoff condition is poor because the directivity for the radial stator is not well predicted. The measured

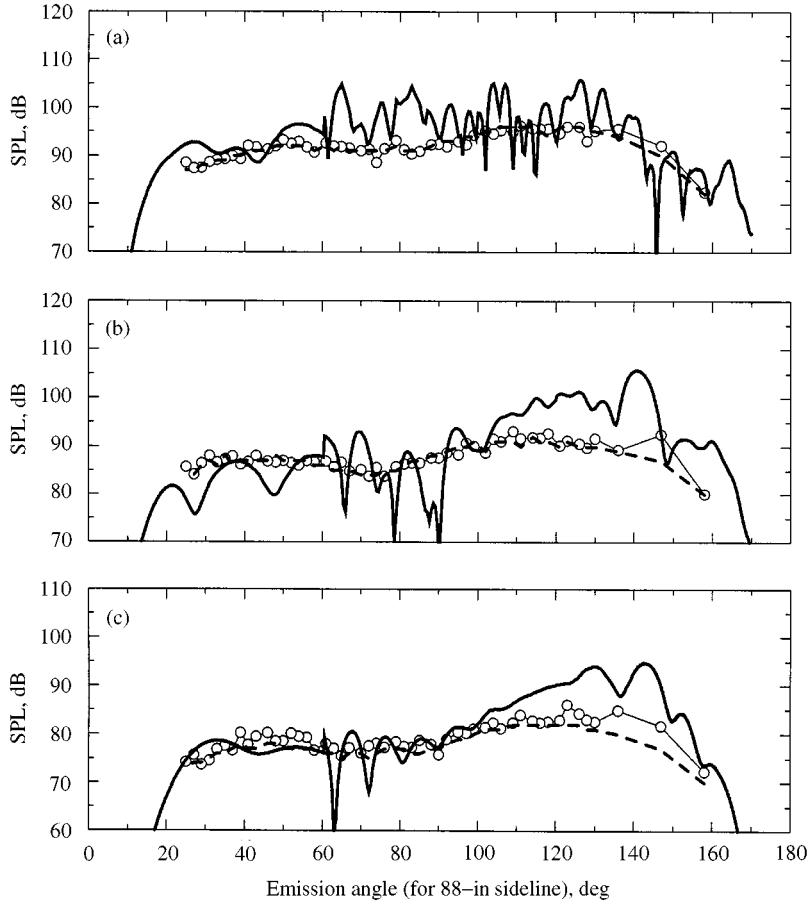

Figure 18. Comparison of measured (symbols) and predicted (solid line) 2BPF tone farfield directivities for the swept and leaned stator. Measured broadband noise level (dashed line) at 2BPF tone is also shown. (a) Shows the takeoff levels, (b) the cutback levels and (c) the approach levels.

reductions are about 5–7 dB for approach and cutback and around 10 dB for takeoff. The predicted reductions are somewhat higher for all three speeds. The tone reductions summarized in Figures 17 and 19 clearly demonstrate the success of sweep and lean in reducing the tone levels and the ability of the theory to capture the essential features of the reductions.

To assess the benefits of swept and leaned stator versus the swept-only stator, the 2BPF tone SPL difference between the two configurations is plotted in Figure 20. Note that the 0-dB line now represents the level due to the swept-only stator. The calculated differences in the measured tone levels are generally centered on the 0-dB level with noticeable additional benefits only in the exhaust region. This suggests that the swept and leaned stator is not significantly quieter than the swept-only stator except in the exhaust. The corresponding predicted differences generally show quite a good agreement for most of the emission angles at all speed

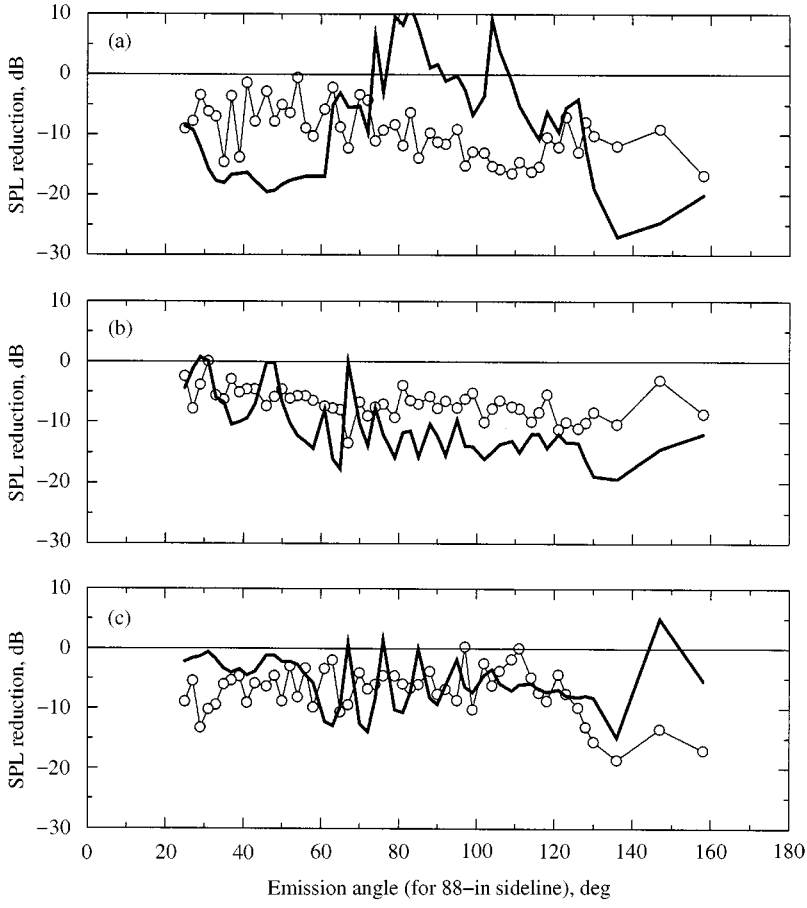

Figure 19. Comparison of measured (symbols) and broadband-corrected predicted (solid line) 2BPF tone reductions in the farfield due to sweep and lean. Radial stator level is the baseline (i.e., 0 dB). (a) Shows the takeoff levels, (b) the cutback levels and (c) the approach levels.

conditions. The exceptions are the predicted benefits for the exhaust emission angles greater than 140° for the cutback and takeoff conditions where the theory predicts significant additional benefits for the swept and leaned OGV compared with the swept-only OGV.

3.2.4. *Radial stator in aft position*

So far, only the comparisons for the radial stator in its nominal (i.e., forward) position have been presented. Next, we present the results and comparisons for the radial stator in its aft position. Recall that for this configuration, the radial stator has the same axial distance from the rotor as the tip of the 30° swept stator. These results are summarized in Figures 21–23. The convention for legends follows those established in the previous figures.

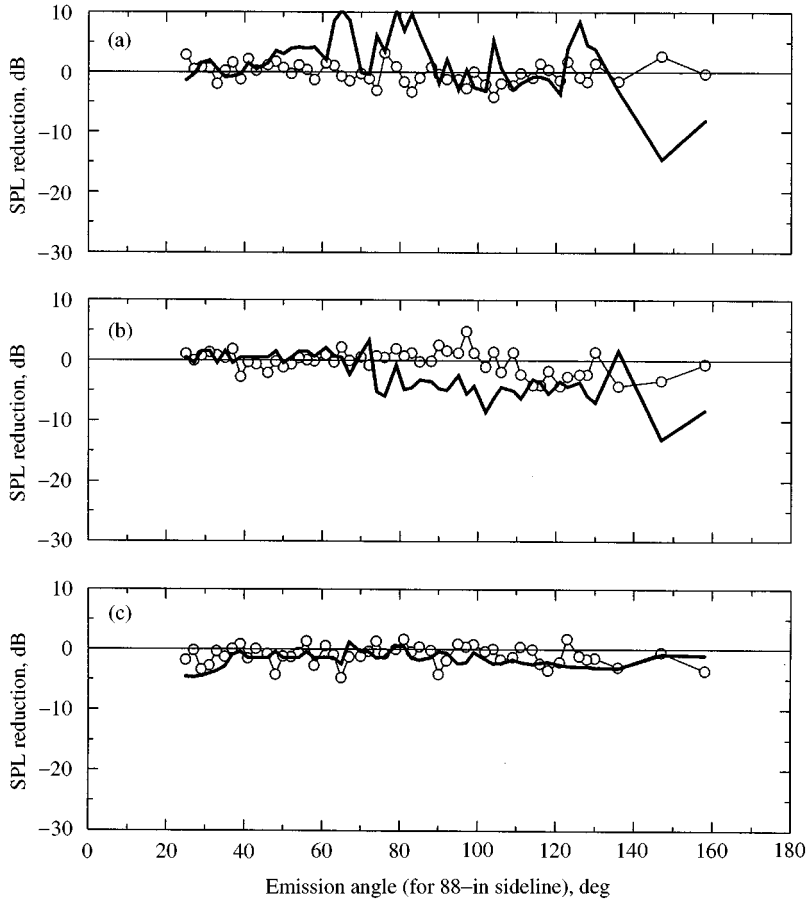

Figure 20. Comparison of measured (symbols) and broadband-corrected predicted (solid line) 2BPF tone reductions in the far field due to sweep and lean. Swept-only stator level is the baseline (i.e., 0 dB). (a) Shows the takeoff levels, (b) the cutback levels and (c) the approach levels.

Figure 21 shows the predicted and measured 2BPF sideline directivities for the radial stator in the aft position. Overall, the directivities (measured and predicted) are very similar to those for the baseline radial stator except that the levels are down by about 5 dB in the data and by around 5–10 dB in the predictions. These reductions are expected because the incident wakes for the radial stator in the aft position are weaker (due to viscous decay) than those for the baseline stator. In addition, there also occurs more wake tilting for the aft-located stator compared to the nominal stator thus further reducing the tone levels.

A comparison of predicted and measured 2BPF noise reductions for the radial stator in the aft position compared with the levels for the baseline radial stator are summarized in Figure 22. In other words, the 0-dB level in this figure corresponds to the noise levels for the radial stator in its nominal (i.e., forward position). Both the broadband-corrected predictions and measured data show roughly 5 dB reductions for all sideline angles at the approach condition. However, the theory

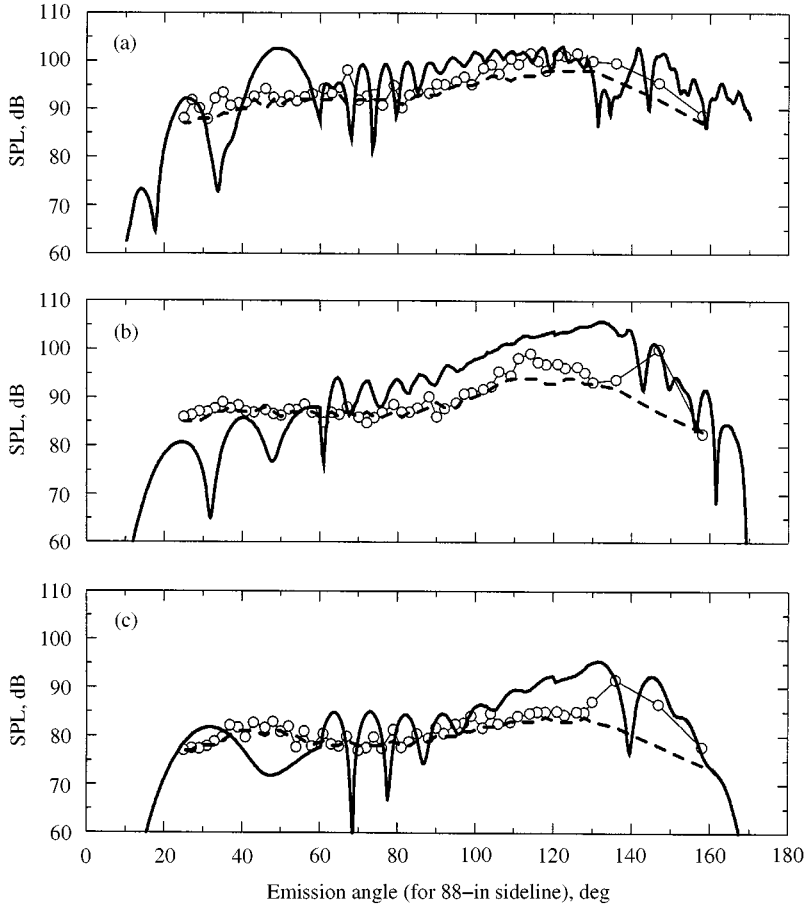

Figure 21. Comparison of measured (symbols) and predicted (solid line) 2BPF tone farfield directivities for the radial stator in the aft axial position. Measured broadband noise level (dashed line) at 2BPF tone is also shown. (a) Shows the takeoff levels, (b) the cutback levels and (c) the approach levels.

predicts somewhat more reductions (around 7 dB) at the cutback condition compared to the data's 5 dB. This is most likely due to the overestimation of the wake viscous decay rate in the theoretical model. Consistent with the earlier results, the data-theory comparison at the takeoff speed is less than satisfactory, with theory predicting roughly 10-dB reduction as compared to the measured 5-dB reductions.

Next, the relative noise benefits of the radial stator in the aft position are compared with those for the swept and leaned stator. The results are summarized in Figure 23. In this figure, the 0-dB level is that due to the radial stator in the aft position and thus reductions here represent additional benefits of sweep and lean that are beyond the axial spacing effects. Generally, both the theory and the measurements show additional reduction due to the sweep and lean compared with the benefits of axial spacing increase. For all three fan speeds, the predicted and

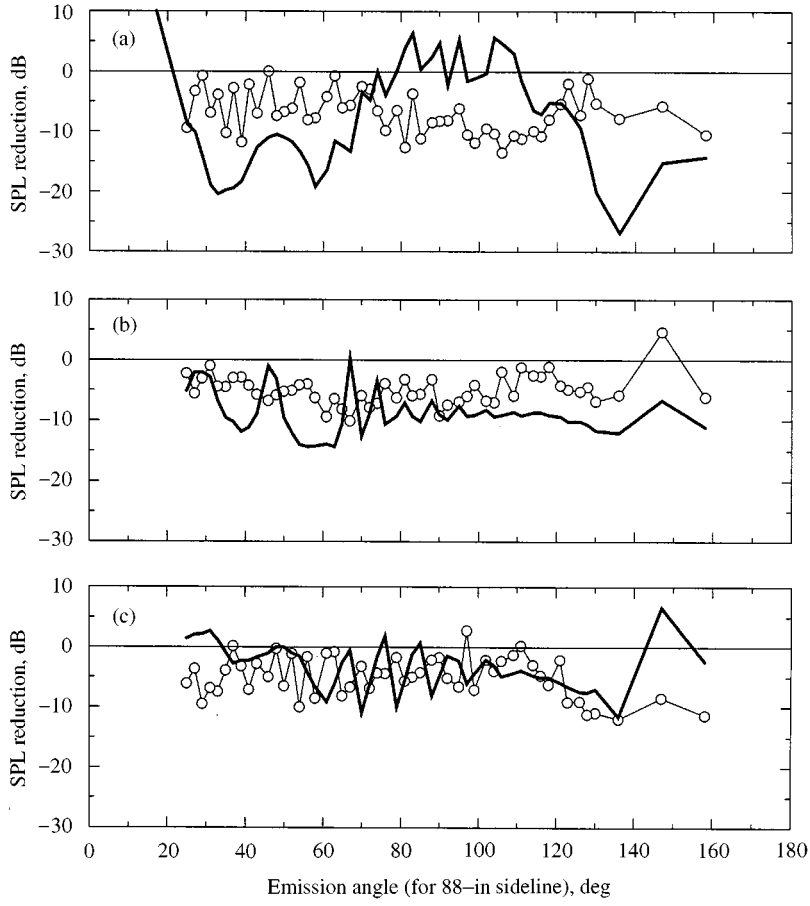

Figure 22. Comparison of measured (symbols) and broadband-corrected predicted (solid line) 2BPF tone reductions in the far field due to axial spacing increase for the radial stator. Nominal radial stator level is the baseline. (a) Shows the takeoff levels, (b) the cutback levels and (c) the approach levels.

measured additional benefits compare rather well. At the approach conditions, both the theory and measurements show that, on the average, there are 2–3 dB of additional benefits due to sweep and lean. The theoretically predicted additional benefits are somewhat larger than the measured ones at the cutback condition. The data show an average of 3 dB of additional benefits, while the theory predicts 4–5 dB. Remarkably, for the takeoff condition, the data-theory comparison is again quite good showing around 5 dB of additional benefits due to sweep and lean. Taken together, these results are in accordance with the conclusions of the design study and clearly show that sweep and lean provide more noise reductions for the same equivalent axial spacing compared with a radial stator.

A tacit assumption used in computing the farfield directivities presented in this report is that the rotor transmission losses are negligible. Despite this approximation, however, the general agreement between the predicted and

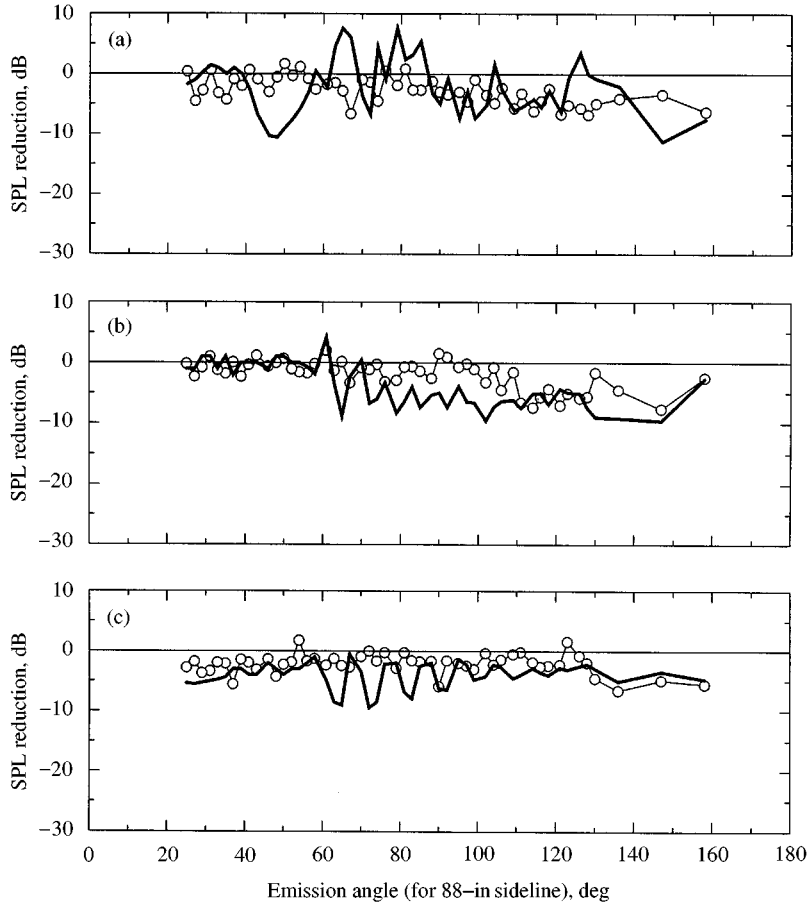

Figure 23. Comparison of measured (symbols) and broadband-corrected predicted (solid line) additional 2BPF tone reductions in the far field due to sweep and lean. The level for the radial stator in the aft position is the baseline. (a) Shows the takeoff levels, (b) the cutback levels and (c) the approach levels.

measured noise reductions is remarkably good. A possible explanation for this agreement is that the 2BPF tone does not suffer significant transmission loss through the rotor for this fan. It is also possible that the rotor affects the absolute levels of the 2BPF tone equally for all three stators, so that it drops out of the difference calculations. However, given that with the exception of the radial stator at the takeoff condition the SPL directivities for all other speeds and configurations are in very good agreement with the data, the first explanation seems more likely.

3.3. SIDELINE DIRECTIVITIES (3BPF RESULTS)

Returning to the data-theory comparisons, we next present the results for the 3BPF tone for which the predictions are restricted to the approach condition only.

The sideline directivities for cutback and takeoff could not be obtained because the mesh resolution requirements for the frequencies corresponding to these conditions are beyond the current capabilities of the two radiation codes. In addition, in the interest of brevity, the 3BPF tone results for the radial stator in the aft position have not been included here. These results follow the trends established for the 2BPF results. Note that, the format of the subsequent presentation is slightly different from the results presented so far.

In Figure 24, measured and predicted 3BPF tone sideline directivities are shown. From the top, the graphs are for the radial, swept-only and swept and leaned stators. The symbols indicate the data and the solid lines represent the predictions. The measured broadband noise level at 3BPF is also shown for each stator (the dashed line). The results indicate that, while there is a reasonably good agreement between the data and theory in the inlet region, there are noticeable underpredictions in the aft region. The magnitude of the underprediction depends

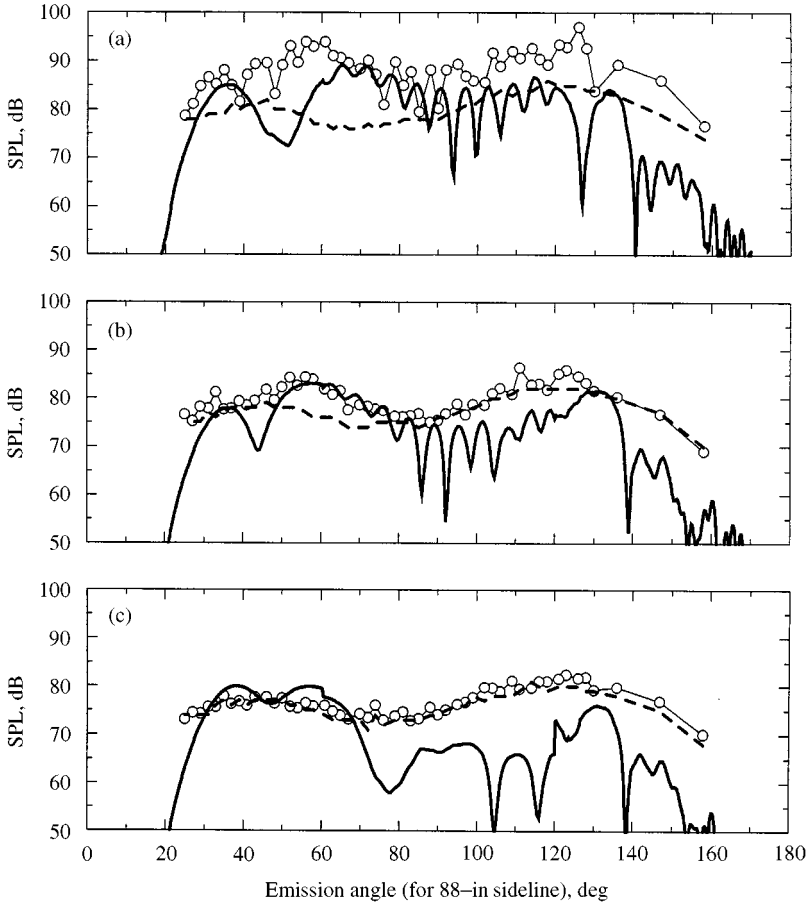

Figure 24. Comparison of measured (symbols) and predicted (solid line) 3BPF tone far field directivities for the (a) radial, (b) swept-only and (c) swept and leaned stators at approach condition. Measured broadband noise level (dashed line) at 3BPF tone is also shown.

on the stator configuration. For the radial and swept-only stators, the discrepancies are modest (around 5 dB), but for the swept and leaned case they are as much as 10 dB. However, it should be noted that, except for the radial case, for which there is noticeable tone protrusion, the levels of measured tone and broadband are virtually equal for the 3BPF tone. Therefore, a better data-theory comparison is obtained when the broadband levels are taken into account in assessing the predicted noise benefits. In that case, the predictions agree rather well with the measured benefits.

In Figure 25, measured and broadband-corrected predicted SPL reductions due to sweep-only and sweep and lean are presented. From the top, the graphs show the noise benefits of a swept-only stator compared with the radial stator (i.e., $p(30, 0) - p(0, 0)$), the benefits of the swept and leaned stator compared with the

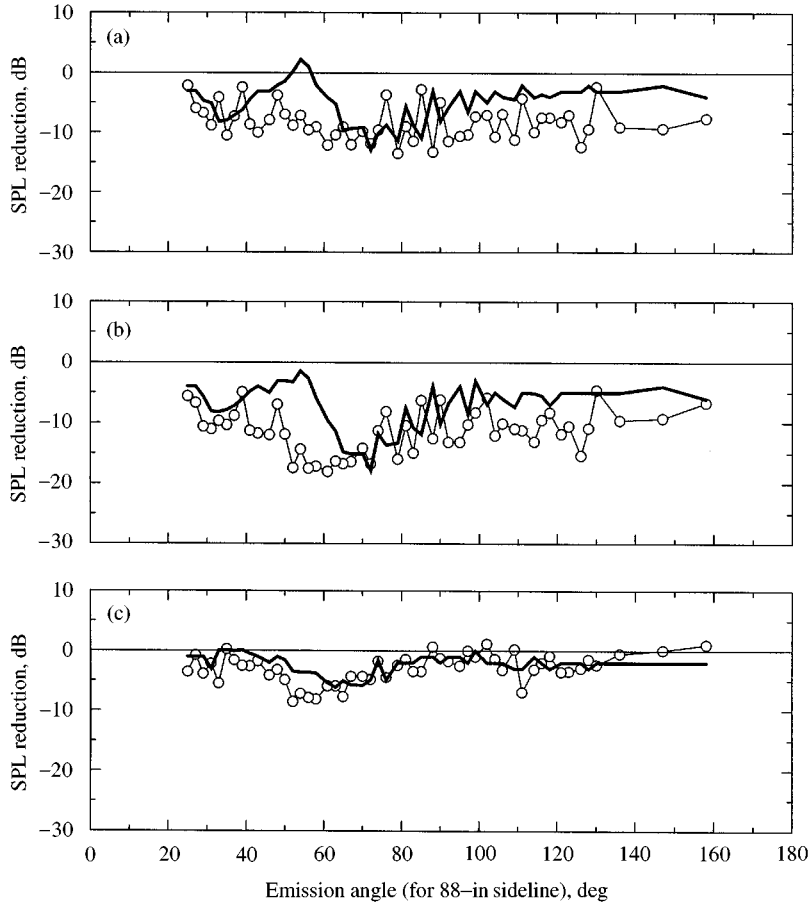

Figure 25. Comparison of measured (symbols) and broadband-corrected predicted (solid line) 3BPF tone reductions in the far field. (a) Shows the sweep-only benefits (i.e., the swept-only stator levels minus the radial stator levels), $p(30, 0) - p(0, 0)$; (b) shows the sweep and lean benefits (i.e., the swept and leaned stator levels minus the radial stator levels) $p(30, -30) - p(0, 0)$; and (c) shows additional benefits of sweep and lean compared with sweep-only benefits (i.e., the swept and leaned stator levels minus the sweep-only stator levels), $p(30, -30) - p(30, 0)$.

radial stator (i.e., $p(30, -30) - p(0, 0)$) and the benefits of the swept and leaned stator compared with the swept-only stator (i.e., $p(30, -30) - p(30, 0)$). Overall, the comparison between the measured reductions (symbols) and the predicted reductions (solid lines) is quite reasonable. Similar to the 2BPF tone, there are measurable noise benefits when the OGV is swept or is swept and leaned in accordance with the predicted in-duct noise reductions shown in Figures 7(b) and 8(b).

3.4. TONE POWER LEVEL COMPARISONS

Since direct data-theory SPL comparisons for higher tone harmonics (and tip speeds) could not be made, an indirect method was employed. The procedure involves comparing the predicted in-duct acoustic power levels with acoustic power level estimates based on integrating the measured sideline SPL for the higher speeds and/or tones. The predicted in-duct power levels were calculated using the BBN/V072 code while the experimental levels were computed by integrating the 1-ft lossless directivities estimated from the measured 88-in sideline SPL. For the sake of consistency and completeness, these comparisons have been carried out at all three speeds and for all the harmonic tones between 2BPF and 5BPF. Using the same procedure, the corresponding broadband noise level in the neighborhood of each tone was also calculated to help with the analysis of the tone data. Only the results for the baseline radial stator, the swept-only and the swept and leaned stator have been computed. The results for the radial stator in the aft position do not alter the main conclusions of this study and, therefore, are not included here.

The absolute tone power levels for the radial stator are shown in Figure 26, those for the swept-only stator in Figure 27 and those for the swept and leaned stator in Figure 28 respectively. In these figures, open bars represent measured levels, solid bars the predicted levels and crosshatched bars the measured broadband levels. The trends with tone order, fan speed and stator configuration are somewhat mixed, but the following observations can be made. The theory overpredicts the levels for the low order tones, especially for the radial stator. The opposite trend is true for the higher order tones particularly for the swept-only and swept and leaned stators. It should be noted that, in the underpredicted cases, the theoretical power level is generally below the measured broadband power level.

In Figures 29–31, the measured reductions (open bars) and broadband-corrected theoretical reductions (solid bars) in the levels of tone power are shown. In computing the broadband-corrected theoretical reductions, the predicted levels themselves were used if they were above the broadband and the broadband levels were used if the predicted theoretical levels were below the broadband level (see Figures 26–28). Figure 29 shows the reductions due to swept-only stator (i.e., $P(30, 0) - P(0, 0)$), Figure 30 the reductions due to swept and leaned stator (i.e., $P(30, -30) - P(0, 0)$) and Figure 31 the reductions due to swept and leaned stator relative to the swept-only stator (i.e., $P(30, -30) - P(30, 0)$). For nearly all combinations of tone harmonic, fan tip speed and sweep and lean, the measured and predicted power level reductions show good agreement. These power level reductions are consistent with the SPL trends shown in section 3.2.

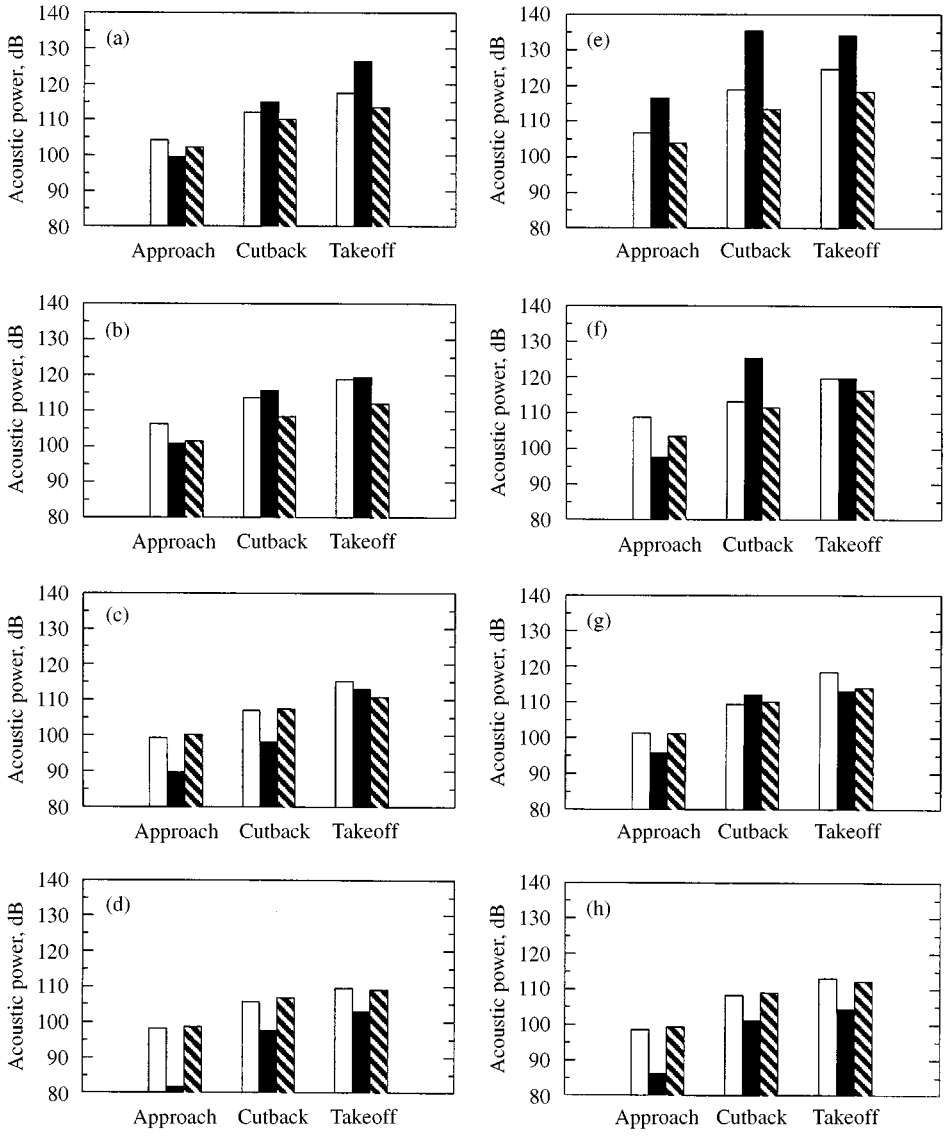

Figure 26. Comparison of measured (open bars) and predicted (solid bars) tone power levels for the nominal radial stator. Broadband power levels (crosshatched bars) in the neighborhood of each tone are also shown. (a) Shows 2BPF upstream levels, (b) 3BPF upstream levels, (c) 4BPF upstream levels, (d) 5BPF upstream levels, (e) 2BPF downstream levels, (f) 3BPF downstream levels, (g) 4BPF downstream levels and (h) 5BPF downstream levels.

4. CONCLUSIONS

A comprehensive two-part analytical study of the benefits of vane sweep and lean for reducing rotor–stator interaction tone noise was presented. The first part summarized a design study aimed at selecting a vane sweep and lean configuration that maximizes the predicted noise reductions for a candidate low-noise stator. The second part focused on a detailed assessment of the acoustic performance of that

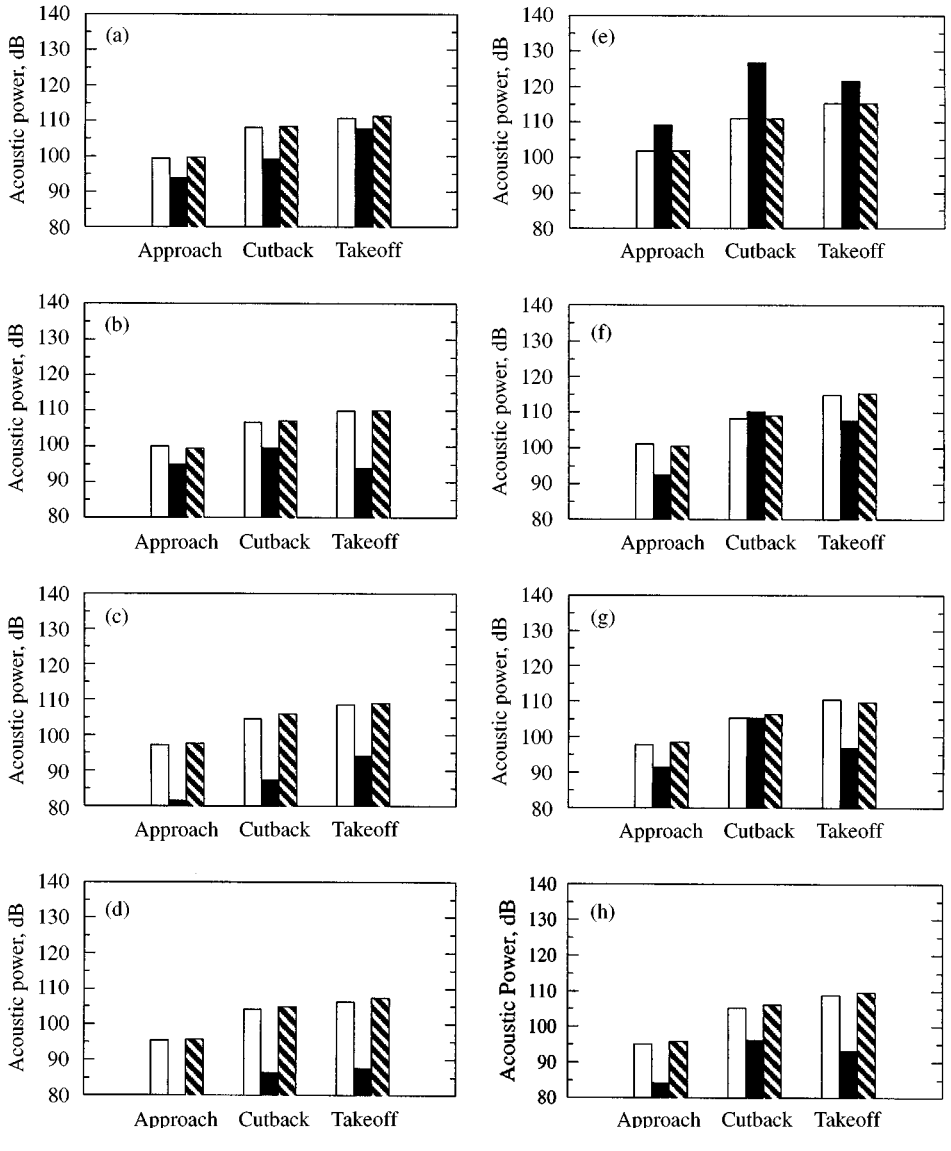

Figure 27. Comparison of measured (open bars) and predicted (solid bars) tone power levels for the swept-only stator. Broadband power levels (crosshatched bars) in the neighborhood of each tone are also shown. (a) Shows 2BPF upstream levels, (b) 3BPF upstream levels, (c) 4BPF upstream levels, (d) 5BPF upstream levels, (e) 2BPF downstream levels, (f) 3BPF downstream levels, (g) 4BPF downstream levels and (h) 5BPF downstream levels.

stator by comparing its predicted noise reductions to its measured benefits and to the performance of alternative low-noise stators.

The main conclusion of this work is that, the kinematic relationship between the rotor wakes and stator vanes is the principal factor in determining the achievable noise reductions due to sweep and lean. In the first part of the study, it was shown that suitable choices for vane sweep and lean enhance wake tilting as seen by the

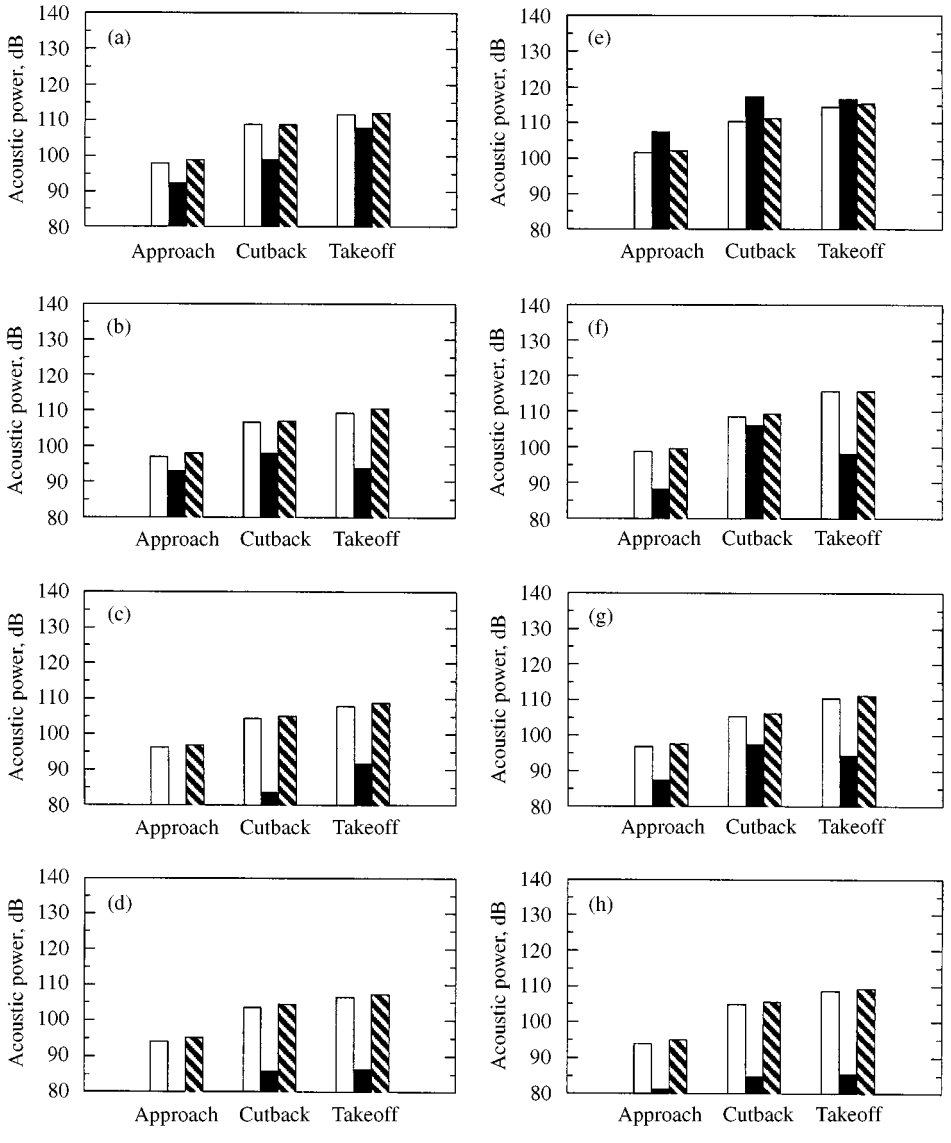

Figure 28. Comparison of measured (open bars) and predicted (solid bars) tone power levels for the swept and leaned stator. Broadband power levels (crosshatched bars) in the neighborhood of each tone are also shown. (a) Shows 2BPF upstream levels, (b) 3BPF upstream levels, (c) 4BPF upstream levels, (d) 5BPF upstream levels, (e) 2BPF downstream levels, (f) 3BPF downstream levels, (g) 4BPF downstream levels and (h) 5BPF downstream levels.

stator, thus increasing the number of wake intersections per vane. An increase in the number of intersections causes significant additional variations in the spanwise phase of the incident wake upwash on the vanes. The net result is the reduction of the tone noise levels for a swept and leaned stator compared with a radial stator. This argument suggests that to reduce noise, sweep and lean must be chosen in such a way that the number of wake intersections per vane is increased. Thus, a simple

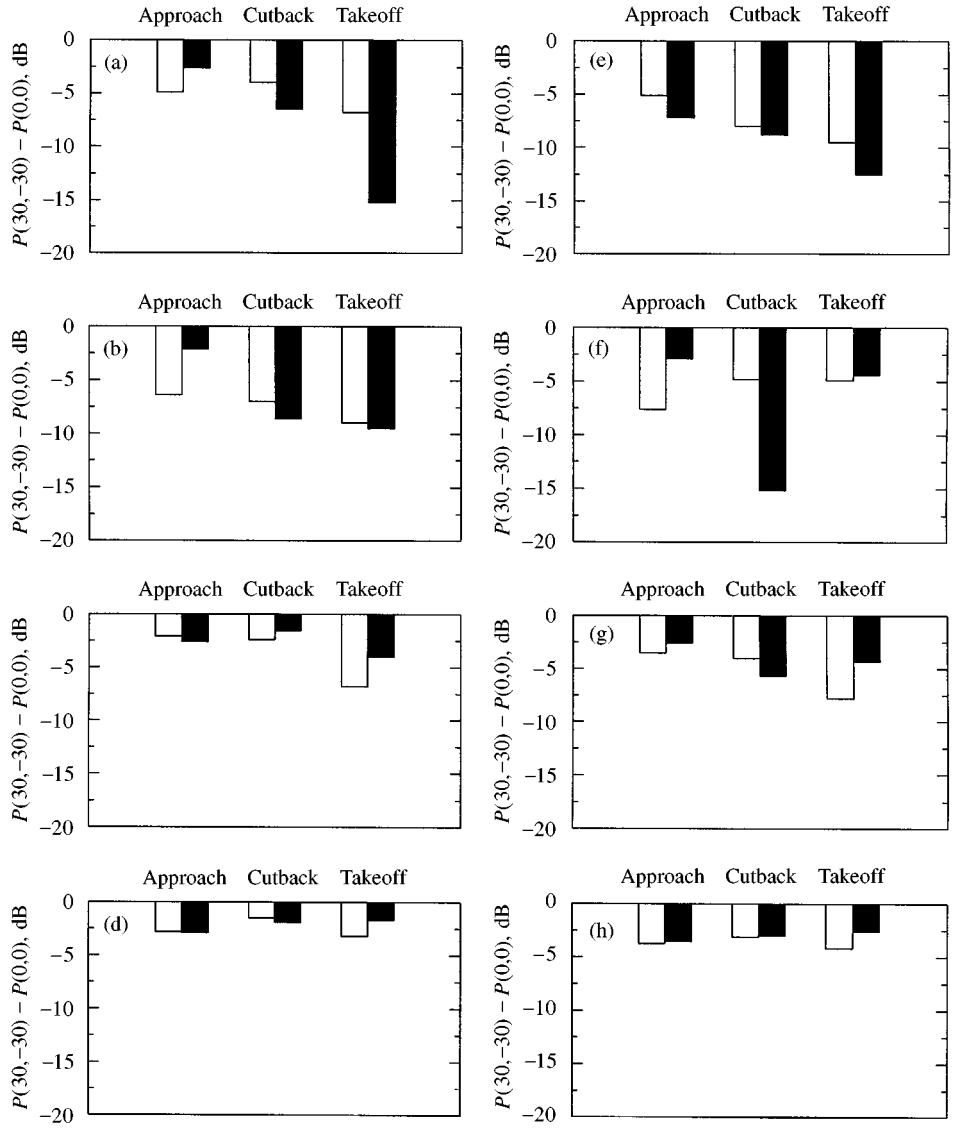

Figure 29. Measured (open bars) and broadband-corrected predicted (solid bars) tone power level reductions for the swept-only stator relative to the radial stator. (a) Shows 2BPF upstream levels, (b) 3BPF downstream levels, (c) 4BPF upstream levels, (d) 5BPF upstream levels, (e) 2BPF downstream levels, (f) 3BPF downstream levels, (g) 4BPF downstream levels and (h) 5BPF downstream levels.

design rule is proposed for implementing sweep and lean in practical fan stages. To achieve noise reductions, the design rule calls for a sweep configuration for which vane tip is downstream of its root. In addition, to enhance the benefits of sweep, the rule calls for vanes that are leaned in the direction of the rotor rotation.

In the second part of the study, the acoustic performance of the swept and leaned stator was compared with the performance of a baseline radial stator as well as those of two other low-noise stators. The comparisons were carried out based on

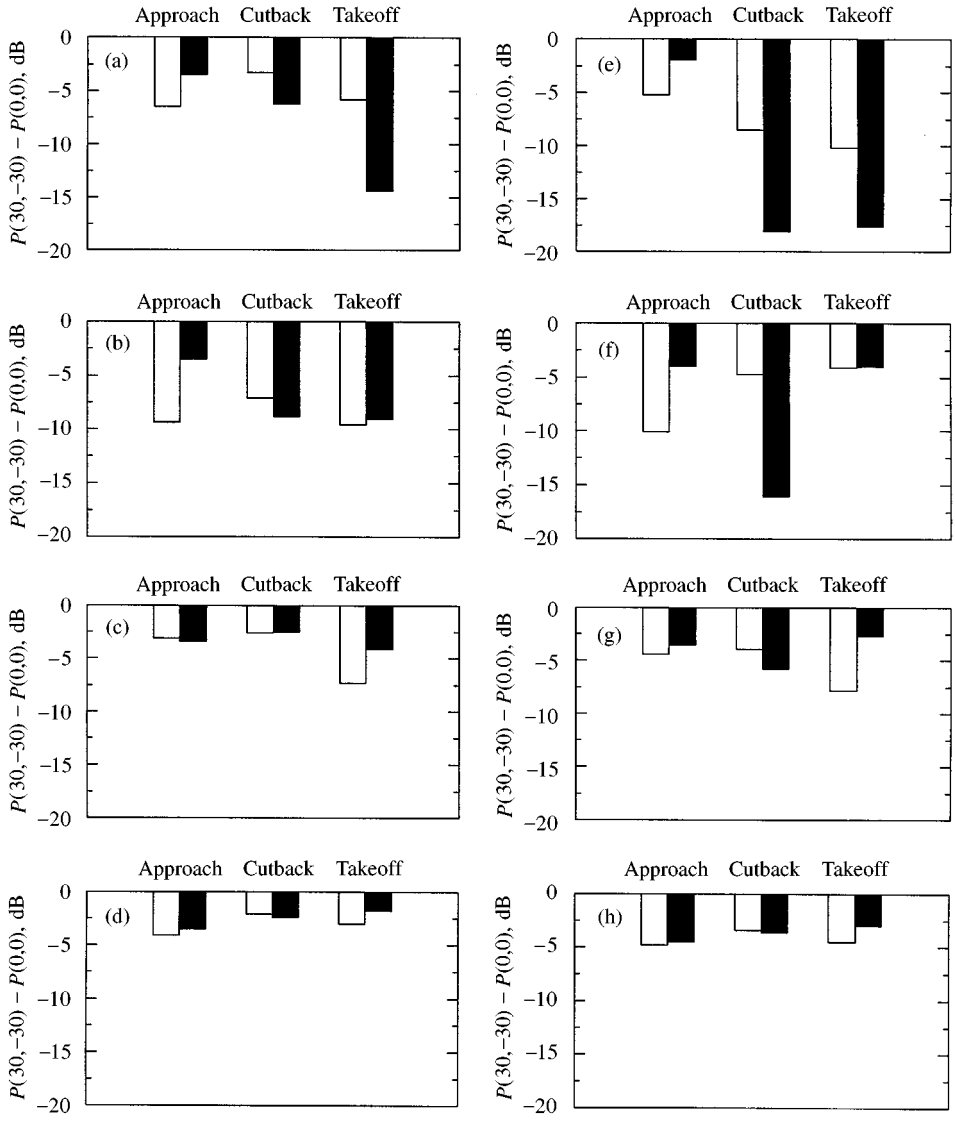

Figure 30. Measured (open bars) and broadband-corrected predicted (solid bars) tone power level reductions for the swept and leaned stator relative to the radial stator. (a) Shows 2BPF upstream levels, (b) 3BPF upstream levels, (c) 4BPF upstream levels, (d) 5BPF upstream levels, (e) 2BPF downstream levels, (f) 3BPF downstream levels, (g) 4BPF downstream levels and (h) 5BPF downstream levels.

the predicted and measured sideline SPL directivities at 2BPF tone and, where available, at 3BPF tone. Additional comparisons for 2BPF through 5BPF tones were also carried out on an acoustic power basis. Overall, the results of these detailed comparisons bear out the validity of the sweep and lean noise reduction concept. Indeed, the results show that the swept and leaned stator is not only significantly quieter than the conventional radial stator, but it is also quieter than both the swept-only and the radial stator in the aft position. This conclusion holds

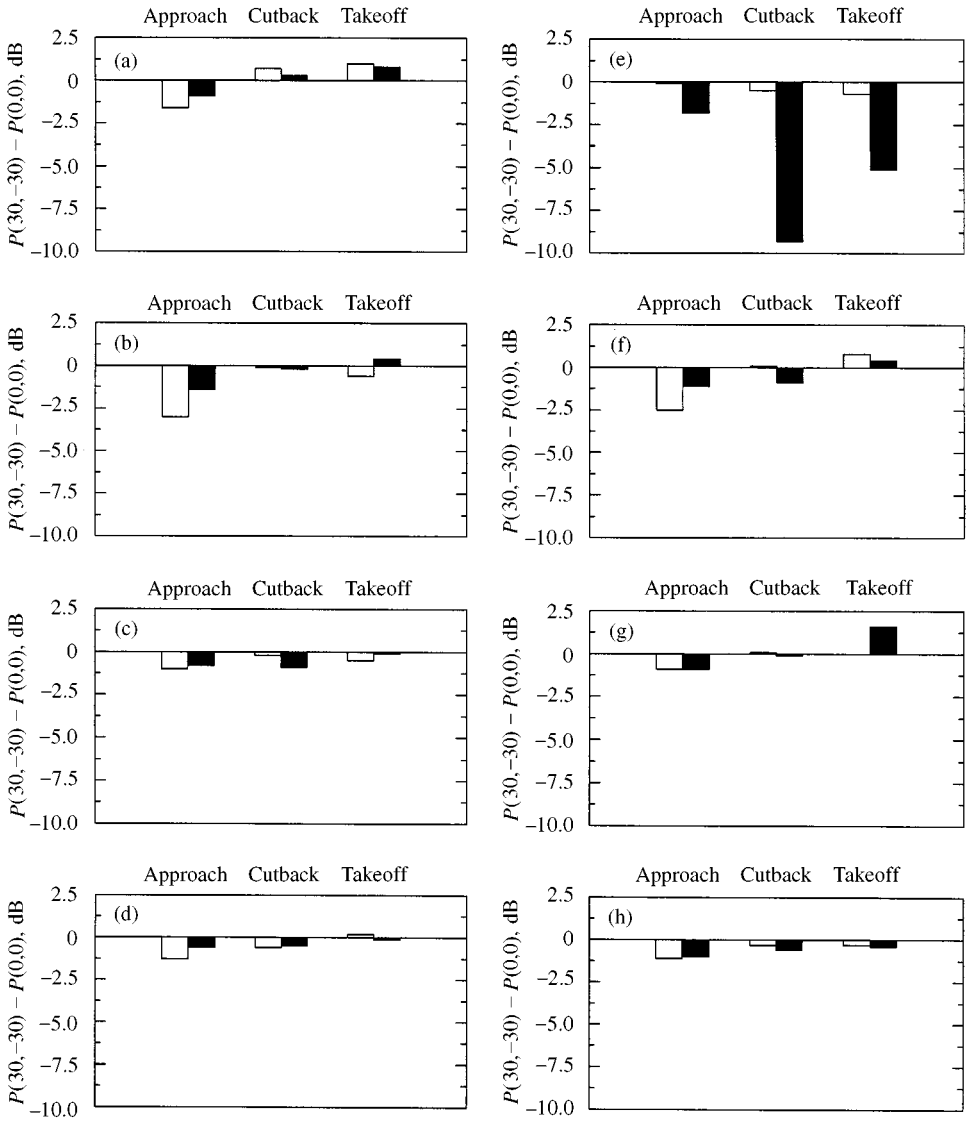

Figure 31. Measured (open bars) and broadband-corrected predicted (solid bars) tone power level reductions for the swept and leaned stator relative to the swept-only stator. (a) Shows 2BPF upstream levels, (b) 3BPF upstream levels, (c) 4BPF upstream levels, (d) 5BPF upstream levels, (e) 2BPF downstream levels, (f) 3BPF downstream levels, (g) 4BPF downstream levels and (h) 5BPF downstream levels.

for all tones and for all three fan speeds considered in this work. Moreover, the predicted noise reductions in nearly all cases show good agreement, qualitative as well as quantitative, with the measured reductions when the broadband noise level is taken into account.

The results from the second part of the study also suggest that the theoretical models used in this work provide reasonably accurate tools for studying the aeroacoustics performance of modern fan stages. It should be emphasized that all of

the theoretical results of this paper were shown without any adjustments or shifts in their levels and as such, they represent true predictions. While accurate prediction of the absolute noise levels for all emission angles (at all fan operating conditions and stator configurations) remains a challenge, the essential features of the farfield SPL directivity, as well as the trends associated with sweep and lean, are accurately captured with the theoretical models used in this study. Improvements in noise source modelling cannot but help enhance the accuracy of these predictions further.

ACKNOWLEDGMENTS

The authors wish to thank Richard P. Woodward and James E. Bridges of NASA Glenn Research Center for providing the acoustic data shown in this report and supplying the routines used for computing the 1-foot lossless acoustic power from the measured SPL directivities. Comments and suggestions of Dennis L. Huff of NASA Glenn Research Center also proved quite valuable.

REFERENCES

1. 1997 *NASA GLENN RESEARCH CENTER MULTIMEDIA CD-ROM* 1997 Quieting the skies: engine noise reduction for subsonic aircraft. (Contact: L. Viterna cto@grc.nasa.gov. or see www.grc.nasa.gov/WWW/AST/noise.htm).
2. J. F. Groeneweg and E. J. Rice 1987 *Transactions of the ASME* **109**, 130–141. Aircraft turbofan noise.
3. G. V. R. Rao 1972 *AIAA Paper* 72-126. Use of leaning vanes for fan noise reduction.
4. S. B. Kazin 1973 *NASA CR*-134486. Radially leaned outlet guide vanes for fan source noise reduction.
5. J. J. Adamczyk 1974 *Journal of Aircraft* **11**, 281–287. Passage of a swept air foil through an oblique gust.
6. R. E. Hayden, D. B. Bliss, B. S. Murray, K. L. Chandiramani, J. I. Smullin and P. G. Schwaar 1977 *NASA CR*-135092. Analysis and design of a high speed, low noise aircraft fan incorporating swept leading edge rotor and stator blades.
7. J. B. H. M. Schulten 1982 *AIAA Journal* **20**, 1352–1358. Sound generated by rotor wakes interacting with a leaned vane stator.
8. E. Envia and E. J. Kerschen 1984 *AIAA Paper* 84-2326. Noise produced by the interaction of a rotor wake with a swept stator blade.
9. E. Envia and E. J. Kerschen 1986 *AIAA Paper* 86-1872. Noise generated by convected gusts interacting with swept airfoil cascdes.
10. E. Envia and E. J. Kerschen 1990 *NASA CR*-187052. Influence of vane sweep on rotor–stator interaction noise.
11. R. P. Woodward, D. M. Elliott, C. E. Hughes and J. J. Berton 1999 *AIAA Paper* 99-0479. Benefits of swept and leaned stators for fan noise reduction.
12. C. S. Ventres, M. A. Theobald and W. D. Mark 1982 *NASA CR*-167951. Turbofan noise generation, Vol. 1: analysis.
13. C. S. Ventres, M. A. Theobald and W. D. Mark 1982 *NASA CR*-167952. Turbofan noise generation, Vol. 2: computer programs.
14. H. D. Meyer and E. Envia 1996 *NASA CR*-4715. Aeroacoustic analysis of turbofan noise generation.
15. D. A. Philbrick and D. A. Topol 1993 *AIAA Paper* 93-4415. Development of a fan noise design system, Part 1: system design and source modeling.

16. R. K. Majjigi and P. R. Gliebe 1984 *NASA CR*-174849, Vol. 1. Development of a rotor/wake vortex model.
17. L. M. Tyler and T. G. Sofrin 1962 *Transactions of SAE* **70**, 309–332. Axial flow compressor noise studies.
18. W. N. Dalton, D. B. Elliott and K. L. Nickols 1999 *NASA CR*-1999-208682. Design of a low speed fan stage.
19. W. Eversman and I. D. Roy 1993 *AIAA Paper* 93-4424. Ducted fan acoustic radiation including the effects of non-uniform mean flow and acoustic treatment.
20. W. Eversman 1995 *AIAA Paper* 95-155. Aft fan duct acoustic radiation.
21. W. Eversman and I. D. Roy 1998 *AIAA Paper* 98-2250. The effect of a baffle on acoustic radiation directivity.
22. D. A. Topol 1993 *AIAA Paper* 93-4416. Development of a fan noise design system, Part 2: farfield radiation and system evaluation.
23. M. Nallasamy 1997 *Journal of Aircraft* **43**, 387–393. Computation of noise radiation from fan inlet and aft ducts.
24. D. L. Sutliff, M. Nallasamy, L. J. Heidelberg and D. M. Elliott 1996 *AIAA Paper* 96-1745. Baseline acoustic levels of the NASA active noise control fan rig.
25. M. Nallasamy, D. L. Sutliff and L. J. Heidelberg 1999 *AIAA Paper* 99-0481. Propagation of spinning acoustic modes in turbofan exhaust ducts.
26. R. P. Woodward, J. H. Dittmar, D. G. Hall and B. Kee-Bowling 1995 *AIAA Paper* 95-0720. Background noise levels measured in the NASA Glenn 9- by 15-foot low-speed wind tunnel.